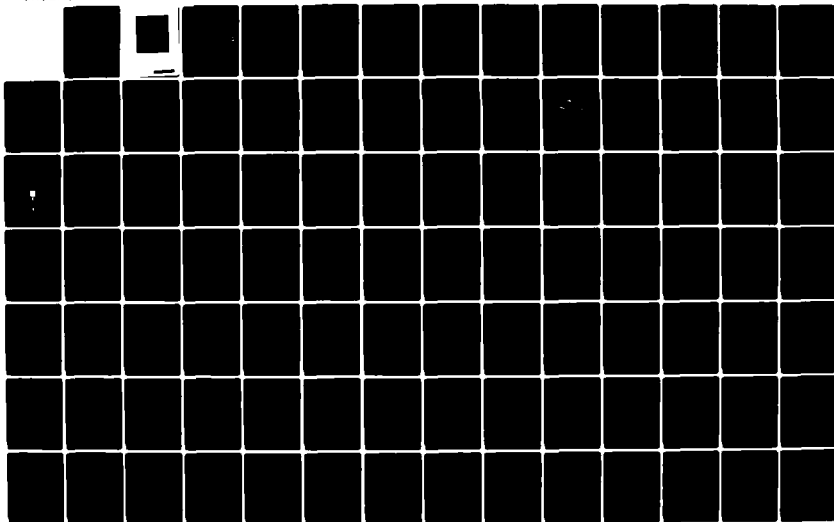AD-A145 431   THE BEHAVIOR OF PB(1-X)SN(X)TE SEMICONDUCTOR LASER   1/2
DIODES IN A MAGNETIC FIELD(U) AIR FORCE INST OF TECH
WRIGHT-PATTERSON AFB OH   G L LORENZEN   MAY 84

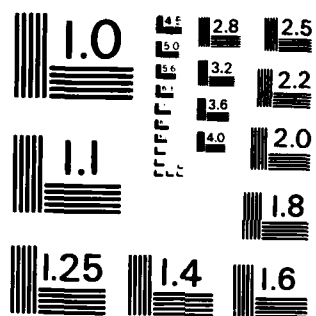UNCLASSIFIED   AFIT/CI/NR-84-42T   F/G 20/12   NL

MICROCOPY RESOLUTION TEST CHART

NATIONAL BUREAU OF STANDARDS - 1963 - A

THE BEHAVIOR OF Pb_{1-x} Sn_x Te SEMICONDUCTOR
LASER DIODES IN A MAGNETIC FIELD

by

Gary Lee Lorenzen

B.S., United States Air Force Academy

(1976)

SUBMITTED IN PARTIAL FULFILLMENT

OF THE REQUIREMENTS OF THE

DEGREE OF

MASTER OF SCIENCE

IN PHYSICS

at the

MASSACHUSETTS INSTITUTE OF TECHNOLOGY

May 1984

REPORT DOCUMENTATION PAGE		READ INSTRUCTIONS BEFORE COMPLETING FORM
1. REPORT NUMBER AFIT/CI/NR 84-42T	2. GOVT ACCESSION NO.	3. RECIPIENT'S CATALOG NUMBER
4. TITLE (and Subtitle) The Behavior of $Pb_{1-x}Sn_xTe$ Semiconductor Laser Diodes in a Magnetic Field		5. TYPE OF REPORT & PERIOD COVERED THESIS/DISSERTATION
		6. PERFORMING ORG. REPORT NUMBER
7. AUTHOR(s) Gary L. Lorenzen		8. CONTRACT OR GRANT NUMBER(s)
9. PERFORMING ORGANIZATION NAME AND ADDRESS AFIT STUDENT AT: Massachusetts Institute of Technology		10. PROGRAM ELEMENT, PROJECT, TASK AREA & WORK UNIT NUMBERS
11. CONTROLLING OFFICE NAME AND ADDRESS AFIT/NR WPAFB OH 45433		12. REPORT DATE May 1984
		13. NUMBER OF PAGES 91
14. MONITORING AGENCY NAME & ADDRESS(if different from Controlling Office)		15. SECURITY CLASS. (of this report) UNCLASS
		15a. DECLASSIFICATION/DOWNGRADING SCHEDULE

16. DISTRIBUTION STATEMENT (of this Report)

APPROVED FOR PUBLIC RELEASE; DISTRIBUTION UNLIMITED

DTIC
ELECTE
SEP 13 1984

B

17. DISTRIBUTION STATEMENT (of the abstract entered in Block 20, if different from Report)

18. SUPPLEMENTARY NOTES

APPROVED FOR PUBLIC RELEASE: IAW AFR 190-1

LYNN E. WOLAVER
Dean for Research and
Professional Development
AFIT, Wright-Patterson AFB OH

19. KEY WORDS (Continue on reverse side if necessary and identify by block number)

20. ABSTRACT (Continue on reverse side if necessary and identify by block number)

ATTACHED

DD $_{1\ JAN\ 73}^{FORM}$ 1473   EDITION OF 1 NOV 65 IS OBSOLETE

UNCLASS

84 09 13 035

AFIT RESEARCH ASSESSMENT

The purpose of this questionnaire is to ascertain the value and/or contribution of research accomplished by students or faculty of the Air Force Institute of Technology (ATC). It would be greatly appreciated if you would complete the following questionnaire and return it to:

AFIT/NR
Wright-Patterson AFB OH 45433

RESEARCH TITLE: __The Behavior of Pb$_{1-x}$Sn$_x$Te Semiconductor Laser Diodes in a Magnetic Field__

AUTHOR: __Gary L. Lorenzen__

RESEARCH ASSESSMENT QUESTIONS:

1. Did this research contribute to a current Air Force project?

( ) a. YES   ( ) b. NO

2. Do you believe this research topic is significant enough that it would have been researched (or contracted) by your organization or another agency if AFIT had not?

( ) a. YES   ( ) b. NO

3. The benefits of AFIT research can often be expressed by the equivalent value that your agency achieved/received by virtue of AFIT performing the research. Can you estimate what this research would have cost if it had been accomplished under contract or if it had been done in-house in terms of manpower and/or dollars?

( ) a. MAN-YEARS _____   ( ) b. $_____

4. Often it is not possible to attach equivalent dollar values to research, although the results of the research may, in fact, be important. Whether or not you were able to establish an equivalent value for this research (3. above), what is your estimate of its significance?

( ) a. HIGHLY   ( ) b. SIGNIFICANT   ( ) c. SLIGHTLY   ( ) d. OF NO
     SIGNIFICANT   SIGNIFICANT   SIGNIFICANCE

5. AFIT welcomes any further comments you may have on the above questions, or any additional details concerning the current application, future potential, or other value of this research. Please use the bottom part of this questionnaire for your statement(s).

NAME   GRADE   POSITION

ORGANIZATION   LOCATION

STATEMENT(s):

THE BEHAVIOR OF $Pb_{1-x}Sn_x Te$ SEMICONDUCTOR
LASER DIODES IN A MAGNETIC FIELD

by

Gary Lee Lorenzen
B.S., United States Air Force Academy
(1976)

SUBMITTED IN PARTIAL FULFILLMENT
OF THE REQUIREMENTS OF THE

DEGREE OF

MASTER OF SCIENCE
IN PHYSICS

at the

MASSACHUSETTS INSTITUTE OF TECHNOLOGY
May 1984

Signature of Author _Gary Lee Lorenzen_
                                            Department of Physics
                                            May 11, 1984

Certified by _Roshan L. Aggarwal_
                                            Roshan L. Aggarwal
                                            Thesis Supervisor

Certified by _Benjamin Lax_
                                            Benjamin Lax
                                            Thesis Supervisor

Accepted by _____

        Chairman, Departmental Committee on Graduate Students

THE BEHAVIOR OF $Pb_{1-x}Sn_xTe$ SEMICONDUCTOR

LASER DIODES IN A MAGNETIC FIELD

by

GARY L. LORENZEN

Submitted to the Department of Physics
on May 11, 1984 in partial fulfillment of the
requirements for the Degree of Master of Science in
Physics

ABSTRACT

This thesis examines the magnetic field behavior of semiconductor laser diodes with $Pb_{1-x}Sn_xTe$ active regions for x values of 0, .14, and .16. Most of the data was taken at temperatures less than $17^\circ K$ with some data taken around $80^\circ K$. The diodes were stripe-mesa diodes with stripe widths from 16 µm to 25 µm and cavity lengths from 317 µm to 355 µm. The four diodes examined included a homojunction, a double heterostructure, a 300 Å quantum well and a 600 Å quantum well laser diode. The frequency at zero magnetic field was plotted as a function of diode current. The average mode separations for the $Pb_{.84}Sn_{.16}Te$ homojunction laser were 1.77 cm^{-1} and 11.44 cm^{-1}. For the PbTe 300 Å quantum well laser at $11^\circ K$ they were 4.92 cm^{-1} and 12.50 cm^{-1}. At $81^\circ K$ the 300 Å quantum well laser had large mode separations (>65 cm^{-1}) which were correlated to theoretical calculations of interband transitions between quantum well energy levels in the conduction band and in the valence band. A magnetic field up to 150 kG was applied along the diode's <100> crystal axis and the relative output power, threshold current and frequency were all plotted as a function of magnetic field strength. For the $Pb_{.84}Sn_{.16}Te$ double heterostructure and the PbTe 600 Å quantum well the output power reached a peak value below a magnetic field strength of 15 kG and never rose above 1/5 of that peak value at stronger fields. The threshold current for $Pb_{.84}Sn_{.16}Te$ homojunction and the PbTe 300 Å quantum well decreased as the magnetic field increased from 7 kG to 50 kG and then increased as the field increased from 70 kG to 150 kG. The frequency increased with magnetic field strength at two different rates. At magnetic field strengths less than 15 kG the frequency increased at a particular rate. Around 15 kG the frequency would drop to near zero field values and start rising at a

slower, near constant rate to field strengths of 150 kG.
This slower rate was .685 cm^{-1}/kG for the $Pb_{.84}Sn_{.16}Te$
homojunction, 1.77 cm^{-1}/kG for the PbTe 300 Å quantum well
and 1.95 cm^{-1}/kG for the PbTe 600 A quantum well.

Thesis Supervisor: Dr. Roshan L. Aggarwal
          Title: Senior Research Scientist

Acknowledgements

TABLE OF CONTENTS

List of Figures

vii

List of Tables

I. INTRODUCTION

Knowledge of the physical factors which determine the behavior of semiconductor lasers is essential for the development of new and improved lasers. This knowledge comes from experiments which examine how the laser behaves as various internal or external factors are changed. Armed with these "how" relationships the theorist can develop or refine the models of laser behavior which enable manufacturers to tailor make lasers with predetermined characteristics. This thesis fits into the experimental part of the above process. The specific focus of the thesis is to examine the behavior of several laser diodes with $Pb_{1-x}Sn_xTe$ active regions as a function of (1) diode current, and (2) strength of an external magnetic field applied perpendicular to the plane of the diode's p-n junction along a < 100 > crystal axis. The thesis is organized into the following sections: Introduction, Experimental Procedure, Experimental Results, and Data Interpretation.

The $Pb_{1-x}Sn_xTe$ semiconductor laser diodes used in this experiment were chips of $Pb_{1-x}Sn_xTe$ (plus other elements) not much larger than grains of table salt. The diodes had p-type substrates onto which n-type layers were grown. The diodes were cleaved perpendicular to the p-n junction in order to obtain a Fabry-Perot cavity. When a forward biasing voltage causes a current, above a certain threshold

value, to flow through the diodes a population inversion is created in the region of the p-n junction. In this region the optical gain is greater than the loss at those frequencies whose energies, $\hbar\omega$, are close to the energy difference between the top of the valence and the bottom of the conduction band. In addition, if the light travels perpendicular to the cleaved end faces at a wavelength for which there is an integral number of half wavelengths between the two end faces, then that light is reinforced by the end face reflections. The portion of the light which is transmitted through the end faces is the laser output from the $Pb_{1-x}Sn_xTe$ diodes which was examined in this experiment.

The frequency of the laser output was measured in this experiment, both as a function of diode current as well as magnetic field strength. When a laser is operating above but near threshold the energy of the laser transition, as mentioned above, is approximately equal to the energy gap (the smallest energy difference between the top of the valence band and the bottom of the conduction band). Thus by measuring the laser frequencies, the energy gap of $Pb_{1-x}Sn_xTe$ can be obtained. As the diode current is increased, other laser frequencies are emitted. If cavity length is known the frequency separations between two adjacent longitudinal modes or Fabry-Peret modes can be used to determine the refractive index of the $Pb_{1-x}Sn_xTe$ material in the active region. Other frequency separations

arise from wave guide behavior within the diode and thus supply clues to the internal structure of the diodes. In quantum well lasers relatively large separations between laser modes may signify transitions between different pairs of conduction and valence band energy levels within the quantum well.

Varying an external magnetic field applied along the <100> crystal axis (perpendicular to the plane of the p-n junction) allows the observation of laser behavior as a function of magnetic field strength. The shift in frequency with magnetic field can be used to determine the effective mass of $Pb_{1-x}Sn_xTe$ as well as the g-factors. In addition to the frequency, the relative output power and the threshold current were also measured as a function of magnetic field strength. The changes in threshold current and the relative output power give clues to the change of the density of states as a function of magnetic field strength.

To obtain the experimental results which can be used to determine the quantities outlined above, the lasers were primarily operated at low temperatures, below $17^{o}K$. The low temperatures help eliminate some of the complications induced by lattice vibrations. They also lower the laser's threshold current. This allows the laser to be operated at high magnetic fields without putting excessive strain on the electrical components in the system. A problem which was of special concern since the diode current was a 150 Hz

square wave. This oscillating diode current allowed the use of a lock in amplifier to improve the signal-to-noise ratio but added the problem of fatigue failure as the current interaction with the magnetic field caused the wires to be pulled and released at 150 Hz.

The magnetic field behavior of $Pb_{1-x}Sn_xTe$ has been examined in the past. In 1966 Butler and Calawa examined PbTe laser diodes at field strengths up to 50 kG.[1] $Pb_{1-x}Sn_xTe$ interband magneto-optical studies were conducted at field strengths up to 100 kG by Smith, Aggarwal, Tao and Lax in 1972[2]. Up to this point I believe that $Pb_{1-x}Sn_xTe$ diode lasers, especially with quantum well structures, have not been studied at constant fields as high as 150 kG. Thus, the results from this experiment should extend the present knowledge of magnetic field behavior in these materials to magnetic field strengths up to 150 kG.

[1] J.F. Butler and A.R. Calawa, "Magnetoemission Studies of PbS, PbTe, and PbSe Diode Lasers" in Physics of Quantum Electronics, ed. by P.L. Kelley, B. Lax, A.F. Tannenwald (McGraw-Hill, New York 1966), p. 458-465.

[2] U. Smith, R.L. Aggarwal, T.F. Tao, B. Lax, "Interband Magneto-Optical Studies in $Pb_{1-x}Sn_xTe$ Alloys," in Physics of IV-VI Compounds and Alloys, ed. by S. Rabii (Gordon and Breach 1974), p. 199-207.

II. EXPERIMENTAL PROCEDURES

A. Introduction

This experiment involved several types of diode lasers with $Pb_{1-x}Sn_xTe$ active regions. Table 1 lists the diodes and some of their characteristics.[3] The lasers are listed

Diode #	Composition of Active Region	Composition of Barriers	Stripe Width	Cavity Length	λ 4-13°K	Laser Type
2	$Pb_{.86}Sn_{.14}Te$	$(Pb_{.86}Sn_{.14})_{.97}Yb_{.03}Te$	25 um		10.7 um	Double Heterostructure
4	$Pb_{.84}Sn_{.16}Te$		22 um	355 um	12.6 um	Homojunction
5	PbTe	$Pb_{.98}Eu_{.02}Se_yTe_{1-y}$	16 um	323 um	6.1 um	300Å Quantum Well
6	PbTe	$Pb_{.98}Eu_{.02}Se_yTe_{1-y}$	23 um	317 um	6.4 um	600Å Quantum Well

Table 1. A list of lasers used in the experiments and some of their characteristics.

by diode number and I will use this number throughout the paper to refer to the diodes. All the diode lasers were made using molecular beam epitaxy and were provided by Dr. Dale Partin of General Motors through Professor Benjamin Lax.

I used the lasers above in two basic setups to collect four types of data. In discussing the experimental procedure I will start with an overall picture of each of these two setups and how they were used. After the overall picture I will discuss the different parts of the setup in more detail. Finally I will conclude the section with the data procedures and initial processing.

---

[3]Diode characteristics (compositions, widths, lengths) provided by Dr. Dale Partin, General Motors Research Labs.

B. Basic Setups

Setup 1, shown in Figure 1, was used to measure how the relative output power of the laser changed as a function of diode current at a fixed magnetic field strength and also as a function of magnetic field strength at fixed diode currents. The measurements of relative output power versus diode current were used to determine the laser's
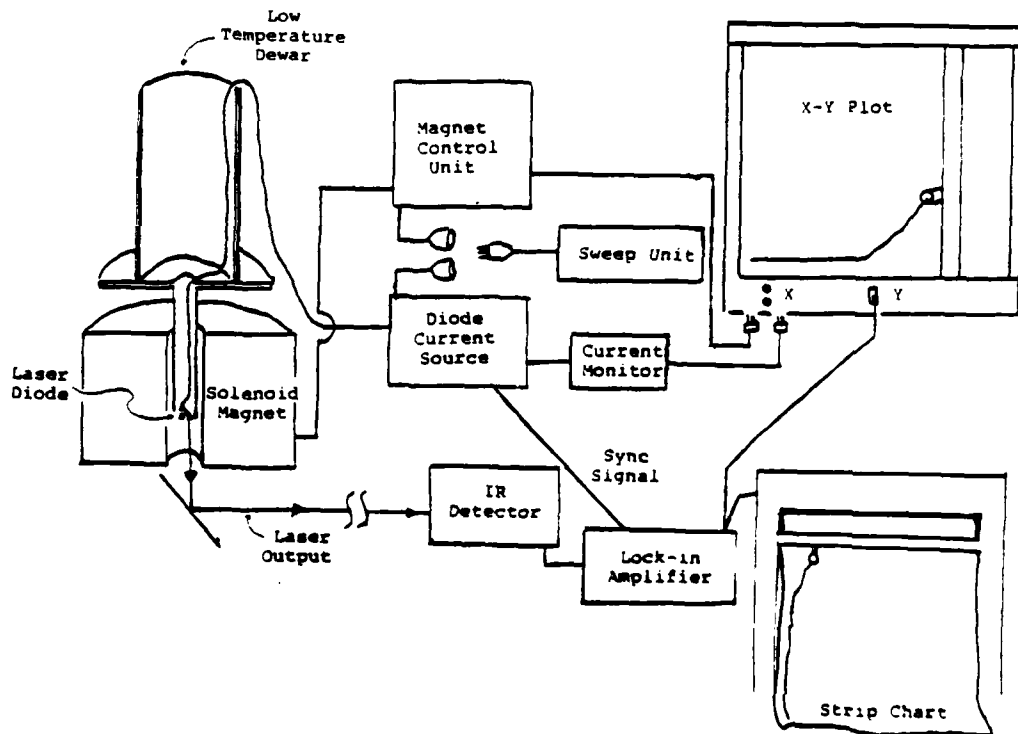

Figure 1. Experimental Setup #1

threshold current. When I took these measurements the sweep unit was connected to the current source to provide a

steadily rising current to the laser. The current monitor
was connected to the X input in the X-Y recorder. The Y
input came from a Princeton Applied Research Model 5101
Lock-in Amplifier which amplified the signals from the
detector which were in synchronization with the current
sent to the laser. The laser itself was mounted on the
cold finger of a low temperature dewar and placed at the
center of a solenoid magnet. When I measured the relative
output power as a function of magnetic field, the sweep
unit was switched from the current source to the magnet
control unit and the X-input of the X-Y recorder was driven
by a monitor output on the magnet control unit. The diode
current was set at a fixed value. The current through the
magnet was then swept from 0 to about 20 kA.

The second basic setup was used to measure the
frequency of the laser both as a function of diode current
and as a function of magnetic field strength. The setup,
as seen in Figure 2, is similar to the first setup except
the sweep unit and X-Y plotter have been removed and a
spectrometer and spectrometer drive unit have been added.
The laser emission was directed through the spectrometer
and then to the IR detector. The detected signal was
amplified and recorded on the strip chart. The magnetic
field and the diode current were set at fixed values and a
spectrometer scan was started simultaneously with the strip
chart drive motor. This produced a chart of peaks which
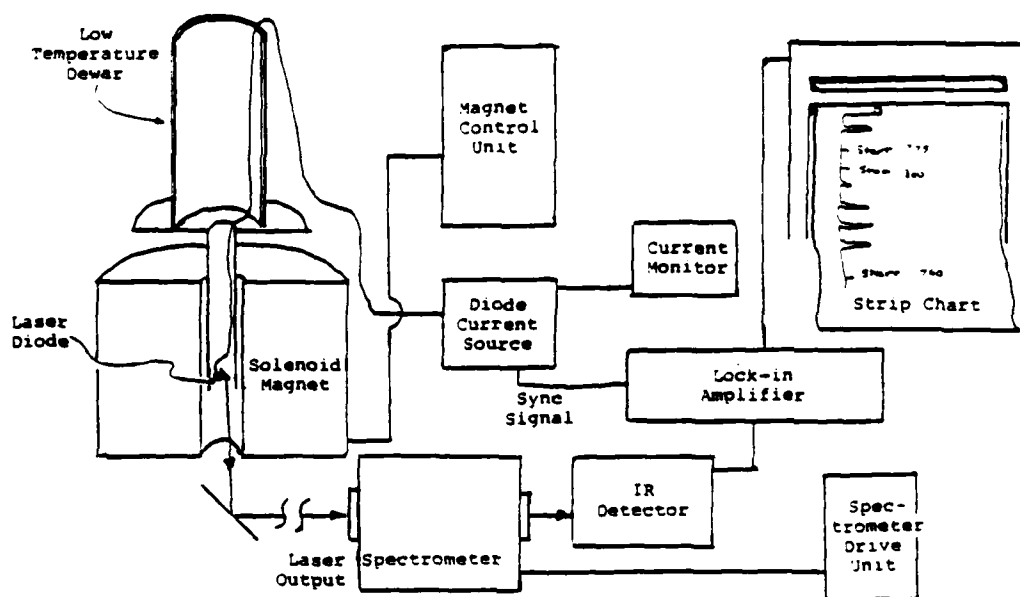
Figure 2.   Experimental Setup #2

corresponded to the laser's emission frequencies.   A   more

thorough description of the data procedures using both of

the   above setups   will follow a detailed   look   at   the

individual parts of the setups.

C.   Equipment Description

In describing the equipment used I will start with the

lasers themselves.   I will then discuss the low temperature

dewar in which the lasers were mounted and current source

which drove the lasers.   After which I will describe the

magnet, the detector, and the spectrometer.

1. Diode Lasers

The lasers themselves were all stripe-configuration diode lasers as shown in Figure 3. The diodes have a
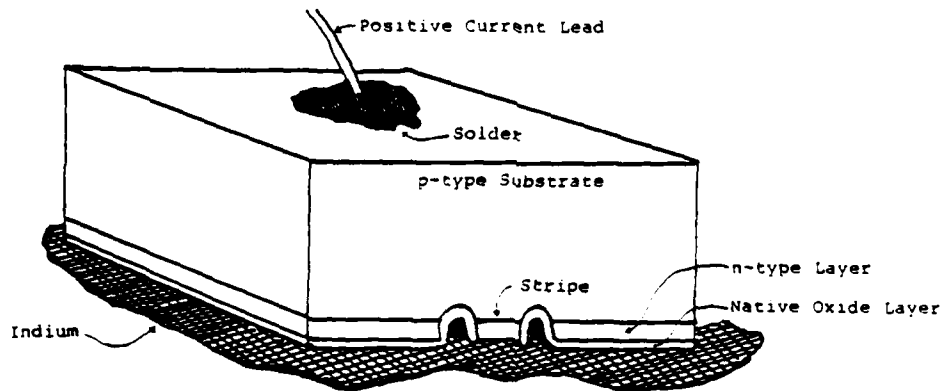
Figure 3. Typical stripe geometry laser (not to scale)

p-type substrate onto which a thin ($\leq .6$ μm) n-type layer was added. Two grooves were cut down the center of the material isolating a central stripe. Only this central stripe was in electrical contact with the pool of indium which physically connected the diode to the copper heat sink. The rest of the n-type layer was insulated from the indium by a native oxide layer.

2. Copper Heat Sink

In Figure 4 the copper heat sink is shown with the diode enlarged for clarity. A positive current lead is soldered to the p-type substrate of the diode and the other
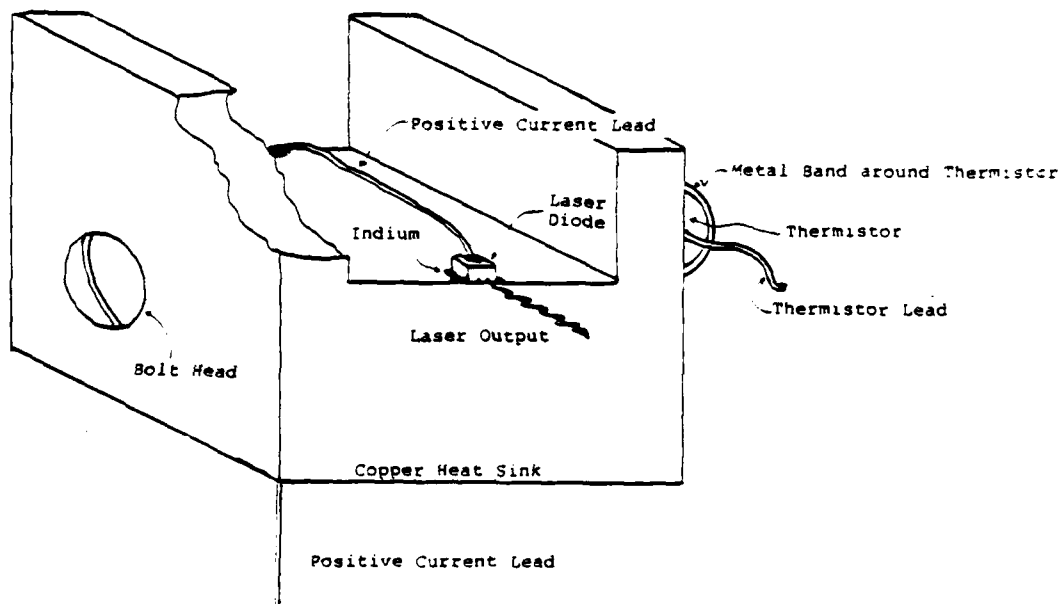
Figure 4.   Laser diode mounted on the copper heat sink.
            The thermistor which is bolted to the copper
            heat sink is partially shown.

end is soldered to the positive lead wire threaded through
the back edge of the copper heat sink.   This lead is
insulated from the copper heat sink which served as the
negative contact for the diode.

3.   Thermistor

During the experiment a thermistor was attached to the
heat sink by wrapping a metal band around the thermistor
and bolting the band to the heat sink.   The thermistor
circuit is shown in Figure 5.   The resistance of the
thermistor varied with the thermistor's temperature.   The
change in the voltage across the thermistor which
corresponded to this change in resistance was read on the
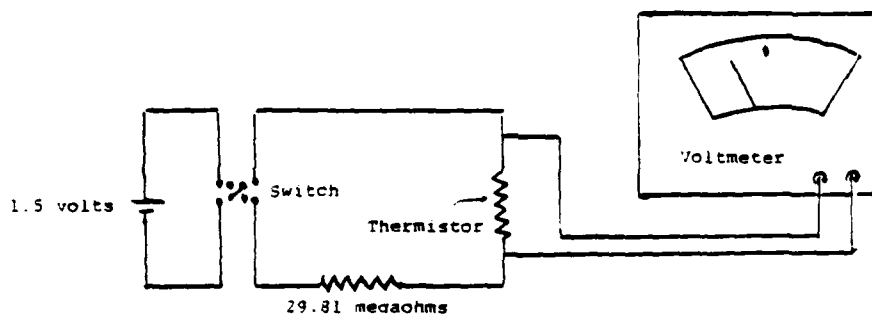
Figure 5. The temperature measuring circuit

voltmeter. The large resistor in the circuit limits the current through the thermistor so it does not heat the heat sink during measurements. The thermistor was calibrated by dipping it into liquid nitrogen and liquid helium. The calibration calculations are in Appendix A.

4. Sample Holder

The copper heat sink with the laser on it was placed on a copper sample holder made to be attached to the end of a cold finger in a low temperature dewar. The laser and heat sink were held in place on the sample holder by two screws and a bar as shown in Figure 6. The negative lead wire was soldered to this bar so the current passed from the diode through the heat sink and to the bar. The laser itself was approximately in the center of the sample holder where the magnetic field was the most uniform. The light emitted from the diode struck the mirror on the sample holder and was reflected down six degrees off the vertical.
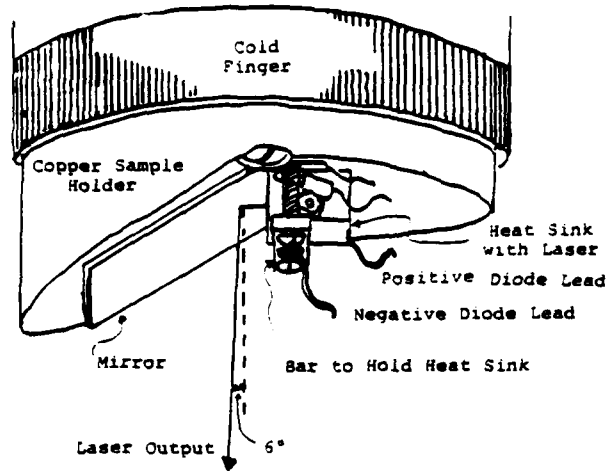
Figure 6.   The heat sink-laser assembly mounted on
the sample holder

5. Low Temperature Dewar

The cold finger on which the sample holder was mounted was part of a Janis Research Company Model 6DT liquid helium dewar with optical access. A cross-section of the dewar, taken from blueprints supplied by the company, is shown in Figure 7. The d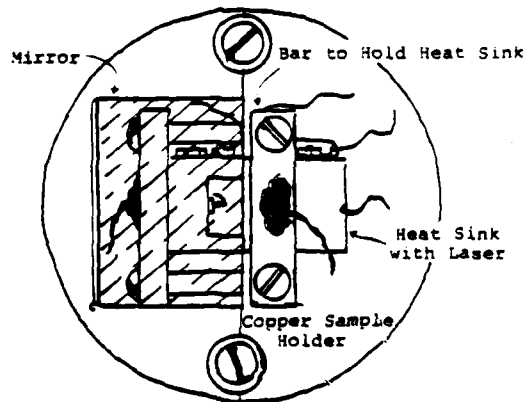ewar was connected to a vacuum pump and a vacuum pressure of at least 5×10^{-5}mm of Hg (usually about 5×10^{-6}mm of Hg) was maintained in the area around the laser. The outer reservoir was filled with liquid nitrogen and the inner reservoir with either liquid helium or liquid nitrogen. The inner reservoir maintained the cold finger temperature and thus the laser's temperature. The positive and negative diode leads and the wires leading to thermistor were wrapped around the inner tail of the dewar and threaded through the vacuum chamber to a connector plug beneath the vacuum valve.

6. Dewar Window

Light from the laser left the dewar through a BaF_2 window on the bottom of the dewar tail. The window thickness was approximately 3 mm. The transmission curve of BaF_2 is shown in Figure 8. This curve was obtained using the actual window in a Perkin Elmer 421 Grating Spectrophotometer. The range of wavelengths involved in this experiment is shown on the curve. The transmission of the window begins to decline at 10 μm. This fact must be

14
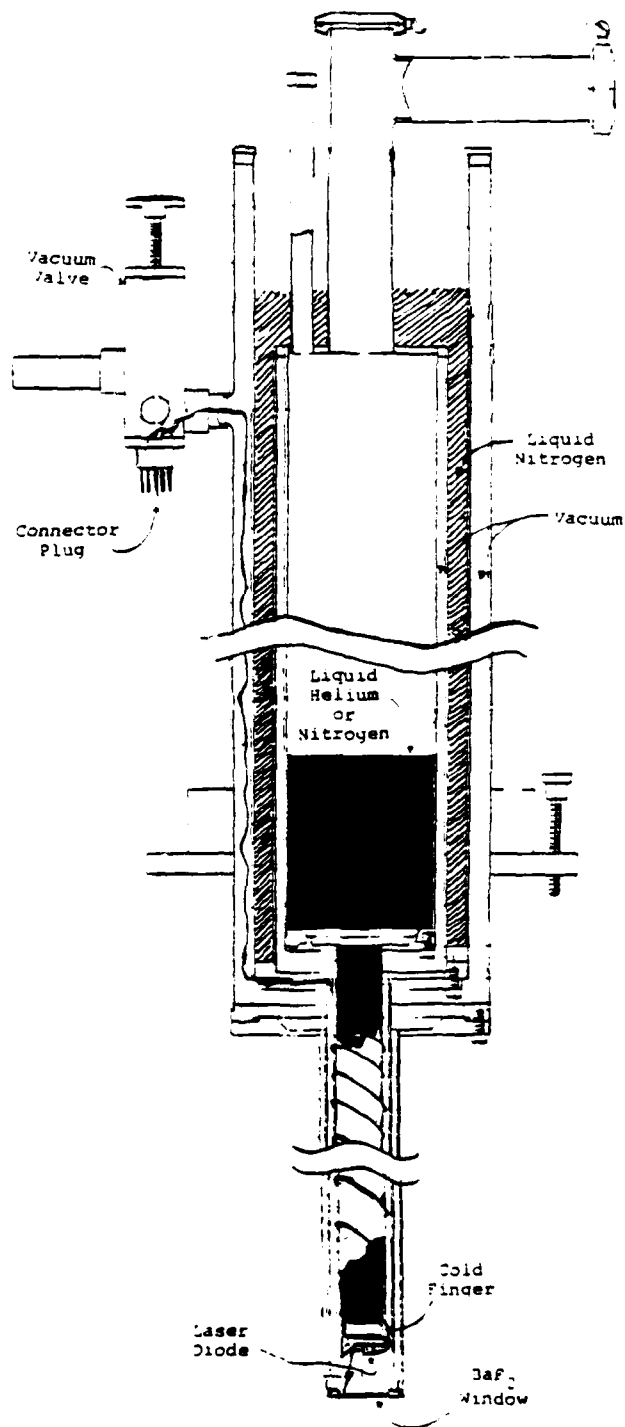
Figure 7. The Janis Research Company Model 6DT Liquid
Helium Dewar with Optical Access
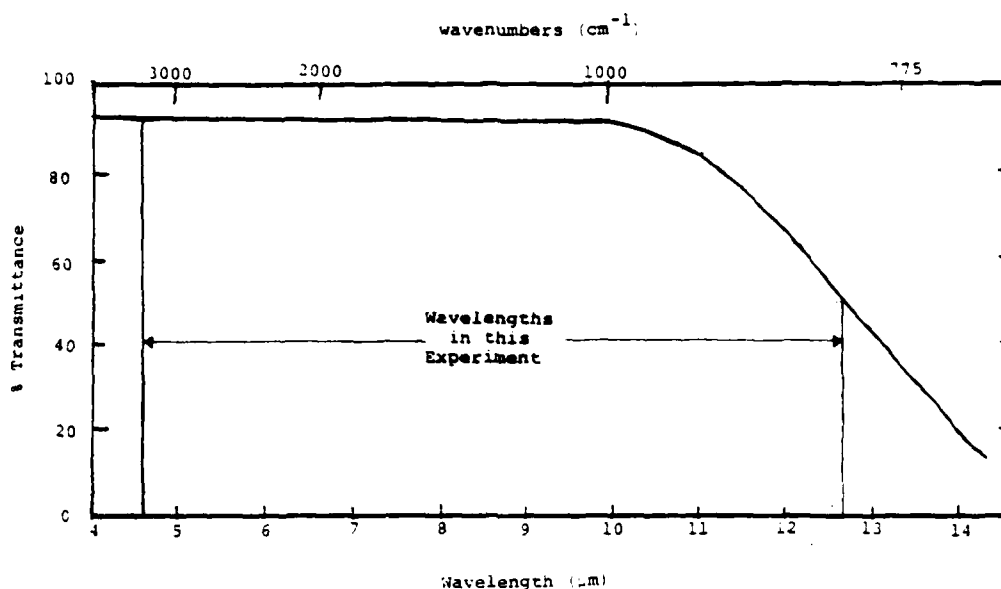
Figure 8. Barium Fluoride transmission curve

considered when interpreting the data. In addition the window itself was not in ideal shape. It had various pits with some as large as 1 mm across which may have attenuated part of the beam.

7. Current Supply

Current was supplied to the laser diode from a current source designed specifically for this experiment. A schematic of this current supply is in Appendix B. Figure 9 is a sketch of the controls to the current supply. The output of the current supply was a fixed or steadily rising or falling 150 Hz, square wave. The square wave rose from zero to a maximum value set by the current level
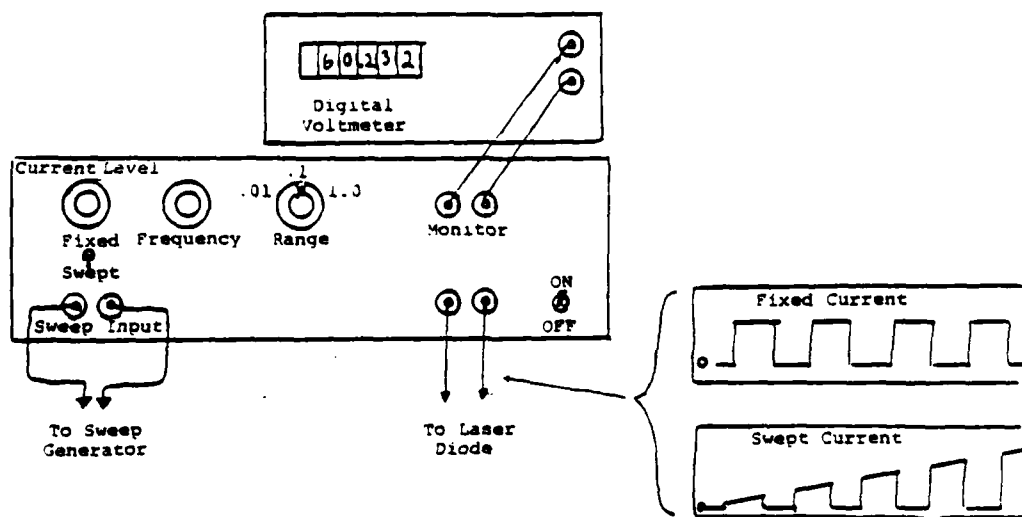
Figure 9. The current source, the current monitor
(digital voltmeter) and two choices of
output current, fixed and swept.

potentiometer or demanded by the sweep voltage driving the
sweep input. It was designed to keep from negatively
biasing the laser diode. The three different ranges of
current available were 0 to 10 mA, 0 to 100 mA and 0 to
1000 mA. A digital voltmeter connected to a monitor output
served as a readout for setting and calibrating the current
supplied to the laser. I calibrated the current source by
measuring the voltage across a standard resistor plugged
into the current output in the place of the laser. The
voltage was compared to a set voltage on a voltage
comparison module of an oscilloscope. Using this method I
could distinguish +.1% of the full scale values on each
scale. A sample calibration is listed in Appendix B.

8. Bitter Magnet

The dewar tail with the laser attached was inserted into the 2 inch bore of a Bitter magnet. The Bitter magnet is a water cooled solenoid magnet. It used up to 20 kA of continuous d.c. current to provide nearly 150 kG of magnet field strength at bore center. Figure 10 is a plot of the magnetic field strength versus the d.c. current through the magnet using data from a typical calibration run. The actual magnet used was the 2S magnet at the Francis Bitter

Figure 10. The magnetic field strength vs. d.c. current.

National Magnet Laboratory, M.I.T. The magnet could be set at any current level from 0-20 kA or swept through the full range using the same sweep unit used to sweep the diode

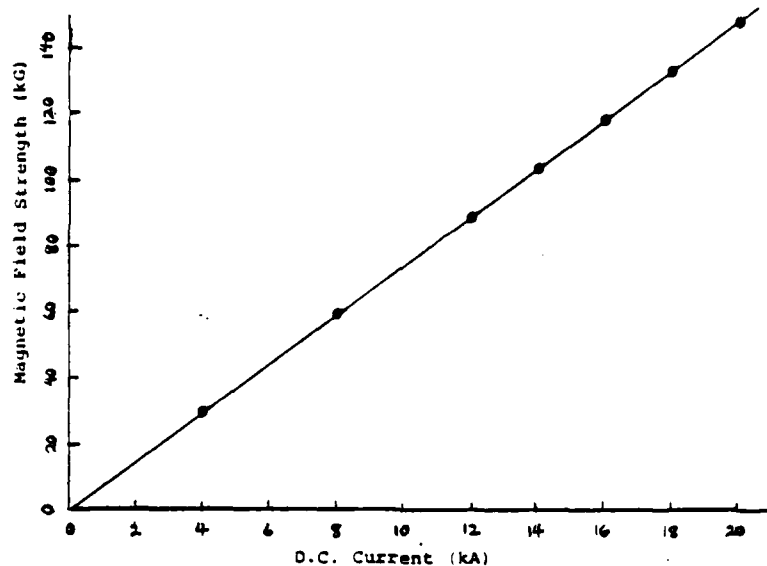current supply. The field strength at each current setting was determined from calibration charts provided by the magnet lab. They were accurate to $\pm.25\%$.

9. Mirror System

Using a system of mirrors the laser output was directed from the magnet bore to either the detector or spectrometer depending on the setup. Figure 11(a) shows a side view of the beam path up to mirror 3. The first mirror was the plane mirror on the sample holder. It directed the beam through the BaF_2 window down past the magnet to mirror 2 at an angle of $6°$ off vertical. Mirror 2 returned the beam to a horizontal path toward mirror 3. Mirror 3 was a spherical mirror with a radius of curvature of 35 in. As seen in the top view in Figure 11(b) mirror 3 was used slightly off axis to direct the beam to mirror 4. The beam came to a focus about 14 in. from mirror 4. The detector was placed back from this point for some of the initial power versus current and power versus magnetic field runs. Mirrors 5 and 6 were added to focus the beam further out and up in order to use the spectrometer. Mirror 5 was a 3 in. spherical mirror with a radius of curvature of 12 in. Mirror 6 was a plane mirror. The spectrometer entrance slit was positioned approximately at focus 2. The detector was also placed back from this focus in the later power versus current or power versus magnetic field runs.
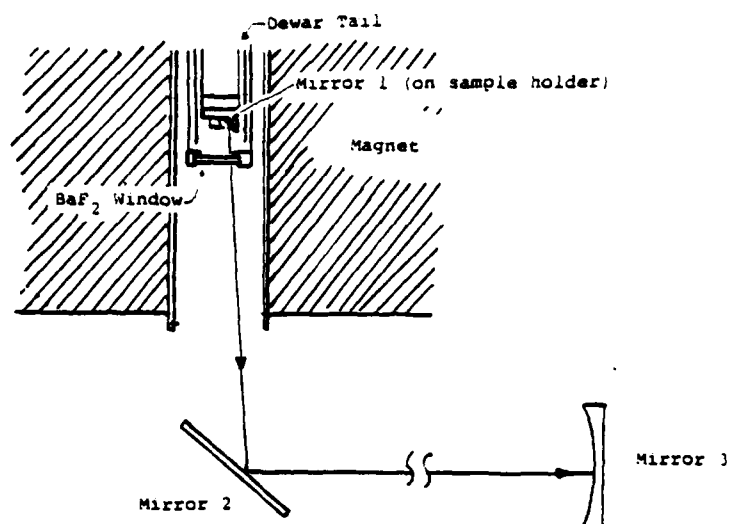
(a) Side View
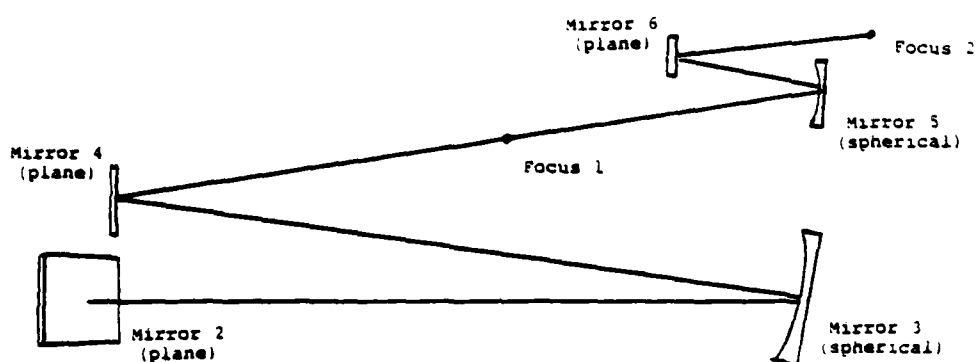
(b) Top View

Figure 11. The mirror arrangement

10. IR Detector

The detector was a copper-doped germanium infrared (IR) detector made by Santa Barbara Research Center. Figure 12 shows the dewar detector configuration and a schematic of the detection circuit. The detector element was mounted in a metal dewar, Model No. 9145-1, designed to be filled with liquid helium for less than $5^{\circ}K$ operation. Between the outside and the detector was a KRS-5 window. A 90° off-axis ellipsoidal mirror mounted beneath the dewar focused the beam on the detector element. In Figure 13 the
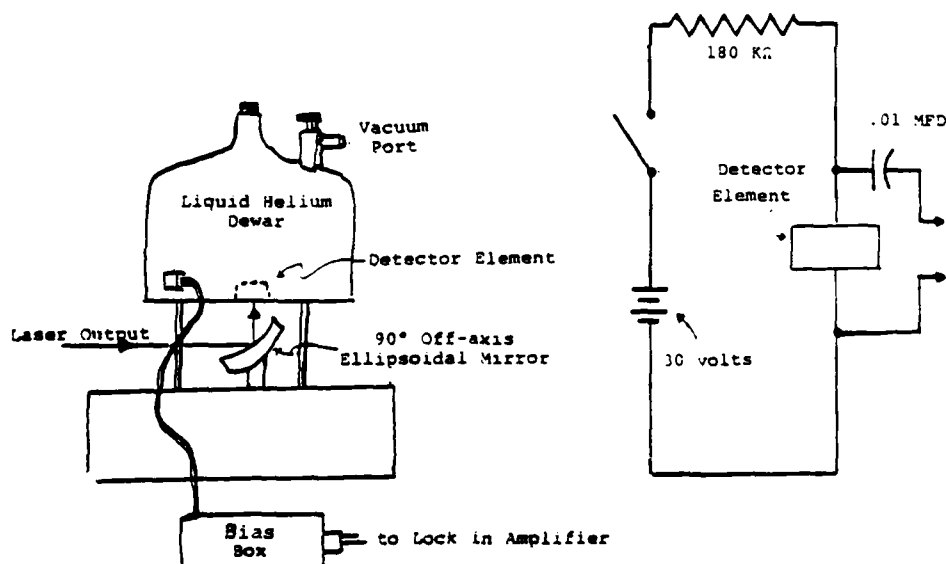
Figure 12. The detector configuration and the detector bias c.rcuit.
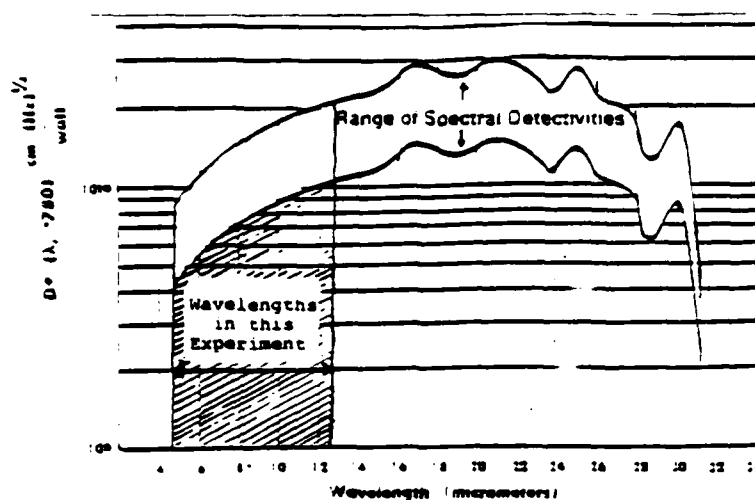
Figure 13. The detector sensitivity

detector's sensitivity curve is shown.[4] The range of
wavelengths measured is marked on the detectivity curve.
The detector was positioned   ∿ 8 in from focus 1 or 2 (see
Figure 10(b)) or the spectrometer exit slits at the point
where it provided maximum detected output.

11. Spectrometer

The spectrometer used in this experiment was Spex
Industries 1680B Spectramate. They describe it as "a high
performance, double monochromator."[5] It contained two 150
gr/mm gratings designed for maximum efficiency at a

---

[4]from the Santa Barbara Research Center Brochure 1980.
[5]1680 Spectramate Instruction, Spex Industries, Inc.© 1976,
p. 1.

wavelength of 10 μm. The gratings were designed so that they move together when scanning. Figure 14, taken from the Spex instruction manual[6], shows the optical layout.

Exit
Slit

Grating 2

Beam Path

Grating 1
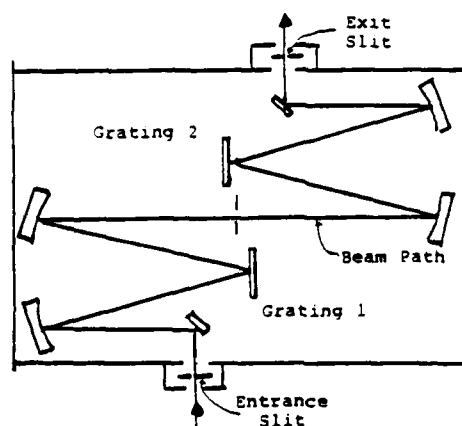
Entrance
Slit

Figure 14. Spex 1680 Spectramate optical layout

The beam path is shown in the figure. The entrance and exit slits are vertical slits and adjustable from 0 to several mm. Most of the data was taken at 100 μm slit width. After the gratings were installed I calibrated the spectrometer at several spectral lines of mercury from a mercury lamp. The unit I used had an external scan controller called an 1673C Minidrive 2. Each time the spectrometer and scan controller were turned on the current

---

[6] *1680* Spex Manual p. 1.

position of the gratings had to be entered into the scan controller. The current grating position was read from the a counter on the end of the spectrometer. The counter read in nanometers of wavelength with tenths of nanometer divisions but was only accurate when using a 1200 gr/mm grating. These readings had to be converted to wavelengths corresponding to the 150 gr/mm gratings and corrected for any errors in grating alignment (observed in calibration). When using laser diodes No. 5 and 6 with wavelengths less than 7 μm the second order mode of the gratings was used and the conversion calculations adjusted accordingly. An outline of the calculations and calibration is in Appendix C. During the experiment a starting and ending wavelengths as well as a scan rate were entered into the scan controller. The scan was started by pushing a button on the scan controller. At the same time I flipped a switch to start the strip chart. I made timing runs of both the spectrometer and the strip chart to correlate their speeds so that distances from the start point on the chart could be converted to wavelengths. Scan rates used primarily were .1 units/sec and .2 units/sec which corresponds to 1.6 nm/sec and 3.2 nm/sec respectively in corrected wavelengths.

The accuracy listed in the specifications[7] was $\pm.4$ nm for a 1200 gr/mm grating with $\pm.2$ nm repeatability. Most of the data was plotted in wavenumbers (cm^{-1}) The above accuracy and repeatability in wavenumbers are $\pm.4$ cm^{-1} and $\pm.2$ cm^{-1} (at 793 cm^{-1} or 12.6 μm) respectively when converted for the 150 gr/mm gratings and corrected for alignment errors. As far as the repeatability, I ran a test using one laser operating in a single mode. After 9 scans I determined a repeatability of $\pm.072$ cm^{-1}. What Spex included in determining their listed accuracy I do not know. The spectrometer counter had tenths of nanometer divisions and could easily be read to .025 nm or about .025 cm^{-1} when setting the scan controller. The error in the scan rate was listed[8] at .18% which would yield $\pm.1$ cm^{-1} error for a five minute scan. A somewhat random error involved how close to "simultaneously" I started the strip chart but my repeatability seems to imply that this error was relatively small.

---

[7] 1680 Spex Manual p. 2.
[8] Operation - Maintenance Instructions: 1673C Minidrive 2 Instructions, Spex Industries, Inc. © 1976, pg. 4-1.

D. Basic Procedures

Having discussed the basic setups and their component parts I will now step through the four basic procedures for taking data. In the first step (Figure 1) mirrors focused the entire spectrum of the laser output on the copper-doped germanium detector. This allowed the measurement of the change in output power, regardless of frequency, as either the diode current or the magnetic field at the laser diode was varied. Varying the diode current produced an X-Y plot of relative output power versus diode current as shown in Figure 15. To produce this chart the current supply was
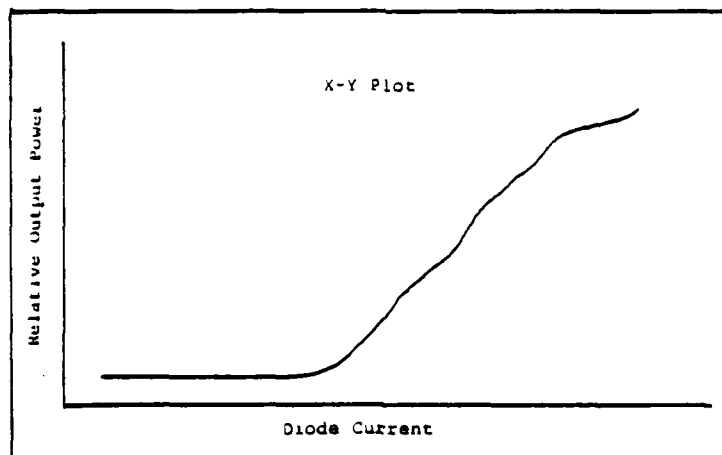
Figure 15. A sample Relative Output Power vs.
Diode Current Chart

set to 0 or some value below threshold and then the sweep generator was started causing the current to slowly

increase. The X-Y plotter was connected to the current monitor and the amplified detector output. The X-Y plots produced were used to determine laser threshold current in two ways. First, if the output power took a sharp rise from zero, a line could be drawn back along the slope to the zero power line as shown in Figure 16(a). The intersection of this line and the zero power line would be called threshold. When the transition into lasing was more gentle a certain arbitrary power level was considered as corresponding to "threshold current" (see Figure 16(b)).

(a) Fast Rise   (b) Slow Rise
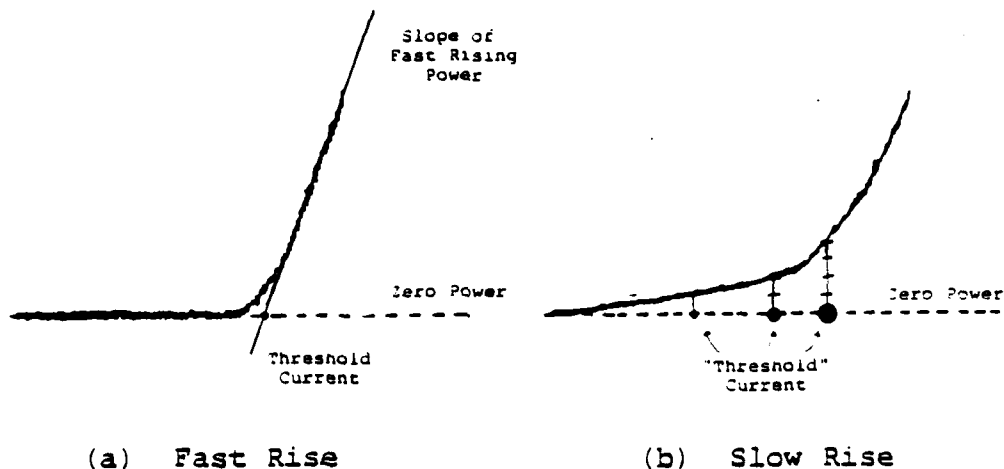
Figure 16. Two ways of determining threshold current

By making X-Y plots like these at various magnetic field strengths I was able to plot the threshold current as a function of magnetic field strength.

Using the same setup, X-Y plots of relative power versus magnetic field strength were made by switching the X

input of the X-Y plotter and the sweep generator to the magnet control unit. The diode current was set at a fixed value. The sweep generator swept the current through the magnet from 0 to approximately 20 kA causing a slowly increasing field from 0 to about 150 kG at the laser diode. A sample chart is shown in Figure 17. For diode No. 4
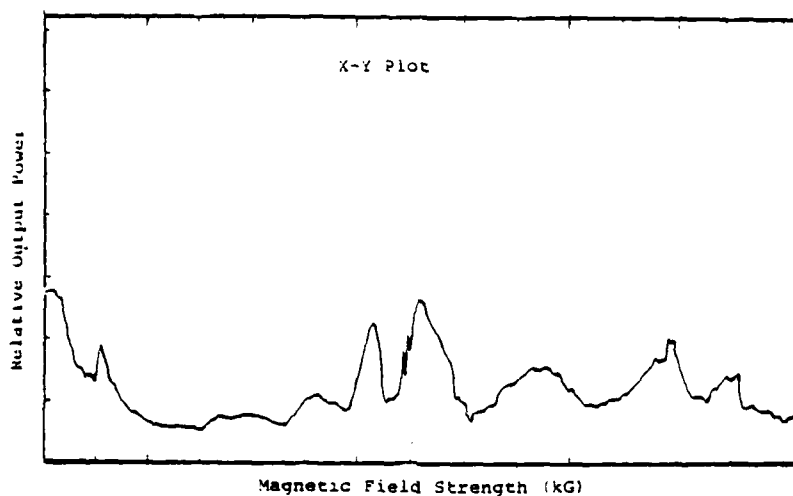
Figure 17. A sample X-Y plot of Relative Output Power vs. Magnetic Field Strength

plots were made at many different diode currents. For the other diodes plots were only made at one or two diode currents (usually the same current used in making the frequency or wavenumber versus magnetic field run.)

The spectrum of the diode was measured using the second basic setup (Figure 2). The laser output was directed through the Spex 1680B Spectramate to the detector. Simultaneously starting the strip chart and the

spectrometer produced a chart as seen in Figure 18. The distance from the start point to a peak corresponded to wavelength difference between starting wavelength and the peak's wavelength. The strip charts were produced at fixed
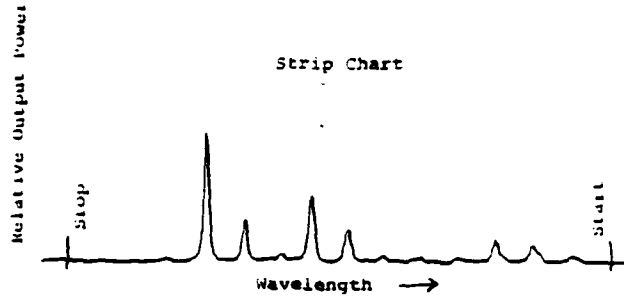
Figure 18. A typical strip chart from a spectrometer scan.

values of magnetic field and diode current. Two types of data were produced. One type involved setting the magnetic field to zero and taking scans at various diode currents from threshold to greater than 40 times threshold current. The other type was produced by setting the diode current well above threshold and taking scans at various magnetic field strengths. The distances to each of the peaks and the peak height were measured on the strip chart for each scan and converted to wavelengths or wavenumbers and peak power. With the help of a personal computer, peaks for each run were tabulated. Each peak's wavenumber was then plotted either as a function of diode current or magnetic field strength depending on the run.

While taking all four types of data the voltage drop across the thermistor (mounted on the laser heat sink) was periodically recorded. The actual laser diode temperature was not known but the thermistor gave a general picture of the temperature during data procedures. When the dewar reservoir was filled with liquid helium the thermistor's voltage drop corresponded to a temperature of $8-16^{\circ}K$ and with liquid nitrogen in the reservoir, it was about $80^{\circ}K$. The thermistor was more sensitive at liquid helium temperatures than it was at liquid nitrogen temperature. At liquid helium temperatures the thermistor registered an increase of usually less than $1^{\circ}K$ in heat sink temperature when operating the diode at high diode currents or strong magnetic fields (the actual measurements made shortly after returning to zero field).

III. EXPERIMENTAL RESULTS

A. Introduction

In this section I will present the results of my experiment. I will start with the laser frequency, $\nu(cm^{-1})$, versus diode current at zero magnetic field. After covering the zero magnetic field result, I will present the magnetic field behavior of each laser. This will include the relative output power, threshold current, and frequency behavior all as a function of magnetic field strength. All the frequency data was taken from strip charts as shown in Figure 18 in the Experimental Procedures section. On those plots which have diode current (mA) as an axis, an alternative scale of current density (kA/cm^2) is provided for those lasers for which the area (stripe width x cavity length) of electrical contact is known.

The diode currents, frequencies, and magnetic field strengths, though plotted without error bars, are not exact. The error in diode current was usually less than ± 1 mA. As discussed in the Experimental Procedures section, the error in frequency is not as well known but was probably less than $\pm .5$ cm^{-1} for absolute frequencies However, the error in the separation between modes depended primarily on the width of the peaks and the errors in the scan rate and strip chart speed. For separations of up to 20 cm^{-1} this error was less than $\pm .2$ cm^{-1}. Finally the

magnetic field strengths were accurate to $\pm.25\%$.

B. Data Presentation

The first plots for each laser are plots of laser frequency in wavenumbers, $\nu(cm^{-1})$, versus diode current in mA. The temperature of the thermistor (or range of temperatures) is recorded on the upper half of each plot. Each diode has a plot at temperatures around $10^{o}K$. In addition, diodes No. 5 and 6 have plots at temperatures around $80^{o}K$. Each frequency mode is represented by a large black dot regardless of its relative output power. I constructed the plots in this way to emphasize the mode patterns and separations. If the frequency separation, $\nabla\nu$, between modes is repeated enough to be clearly identified, then the average separation, $\overline{\nabla\nu}$, is printed in the upper left corner of the plot. If there are two different repeated separations then they are both listed.

After each laser's zero field frequency versus diode current data the magnetic field data is presented. All of the lasers were placed in a magnetic field. The field was applied perpendicular to the p-n junction along the 100 crystal axis pointing from the p-type region to the n-type layer. The presentation of magnetic field data for each laser usually took two pages. One page has the plots for relative output power versus magnetic field and for the threshold current versus magnetic field. The following

page has the frequency versus magnetic field behavior. For diode No. 5 the threshold current was measured as a function of magnetic field both with liquid helium in the dewar's inner reservoir and with liquid nitrogen in the reservoir. Both plots are shown. I will describe each of the types of plots in more detail and then prior to each diode's data I will mention any pertinent comments for the particular diode.

The relative output power versus magnetic field strength is the first plot for each diode of the magnetic field data. As explained in the Experimental Procedures section, this X-Y plot was produced by sweeping the magnetic field while plotting the detector output. Though only one is shown, for many of these plots both the sweep up in field strength and the sweep down were plotted. The up and down plots were virtually identical. Thus, the data should be very reproducible. The fixed current through the diode is listed on each plot. For diode No. 4 a variety of diode currents were plotted but only the one with the same diode current as used in the frequency versus magnetic field plot is displayed. (The plots of other current values were similar in general form with most of the major peaks being repeated.) The relative power units are arbitrary and cannot be compared from diode to diode. In addition when the wavelengths are between 10 μm and 12.6 μm (or wavenumbers less 1000 cm^{-1}) the selective transmission of the BaF_2 window must be taken into consideration when

examining the relative output power versus magnetic field chart. The magnetic field strengths were computed by marking several calibration points on a chart and interpolated from those points. As mentioned earlier the magnetic field strengths were accurate to $\pm.25\%$.

Below the relative power versus magnetic field plot is the threshold current versus magnetic field plot. Some of these were plotted using an arbitrary output power level as "threshold." This was explained in the Experimental Procedures section. These plots often have two or three different symbols at each magnetic field setting. The different symbols correspond to different signal to noise ratios and are plotted to indicate the steepness in the rise of the relative power versus current plot from which the data was taken.

The final chart shows the spectrum change with magnetic field. Each dot on the chart represents a individual mode which the laser emitted. The squares are the centers of power for each field strength. These were computed by multiplying each mode's frequency by the relative power for that mode and then dividing the sum of those values by the total power at that magnetic field strength. At the lower fields often two centers of powers were computed at each field strength, an upper and lower center. For most of the plots these centers of power formed two lines of different slopes. The upper line

seemed to reach a cutoff point at low fields (<30 kG) and the lines through those centers of power are just eyeball guesses. The lower line however is the least squares fit of the centers of power along the straight portion of the line. The slope of the lower line was listed on the plot.

1. Laser Diode No. 4

Laser Diode No. 4 is a homojunction stripe-configured diode laser. It has a 355 µm cavity length and a stripe width of 22 µm for a stripe surface area of $7.81 \times 10^{-5} cm^2$. The laser is made of $Pb_{.84}Sn_{.16}Te$. The first plot is the frequency versus diode current, as seen in Figure 19. This plot shows that the laser operated in a single mode up to about 180 mA of diode current (2.3 kA/cm^2) and then split into many modes. Two separations were often repeated. The smaller average separation, $\overline{\nabla\nu}_1$, equaled 1.77 cm^{-1} and the longer, $\overline{\nu}_2$, equaled 11.44 cm^{-1}.

Figures 20 and 21 illustrate the magnetic field behavior of diode No. 4. The top half of Figure 20 is the plot of relative output power versus magnetic field strength. Since the wavelength changed with magnetic field from 12.6 µm to 11.3 µm (see Figures 21) the relative output power plot must be adjusted to account for the wavelength dependent transmission of the BaF_2's window (see Figure 8). From 12.6 µm to 11.3 µm BaF_2 transmittance goes approximately linearly from 50% to 77%.

The bottom half of Figure 20 is the threshold current versus magnetic field plot. The three points at zero magnetic field were taken at different times. The lowest point was taken first. After taking data through 50 kG the second point was taken. Finally after the rest of the data

was taken the third point up was taken. The slow increase in threshold was probably due to an increase in diode temperature due to the magnetic field.

Figure 21 is a plot of the frequency, in wavenumbers (cm^{-1}), versus magnetic field strength at 80 mA diode current. The slope of the least squares fit lower line was .685 cm^{-1}/kG as indicated on the figure. Though not shown, plots were also made at diode currents of 60 mA and 100 mA and their slopes were .685 cm^{-1}/kG and .672 cm^{-1}/kG respectively.
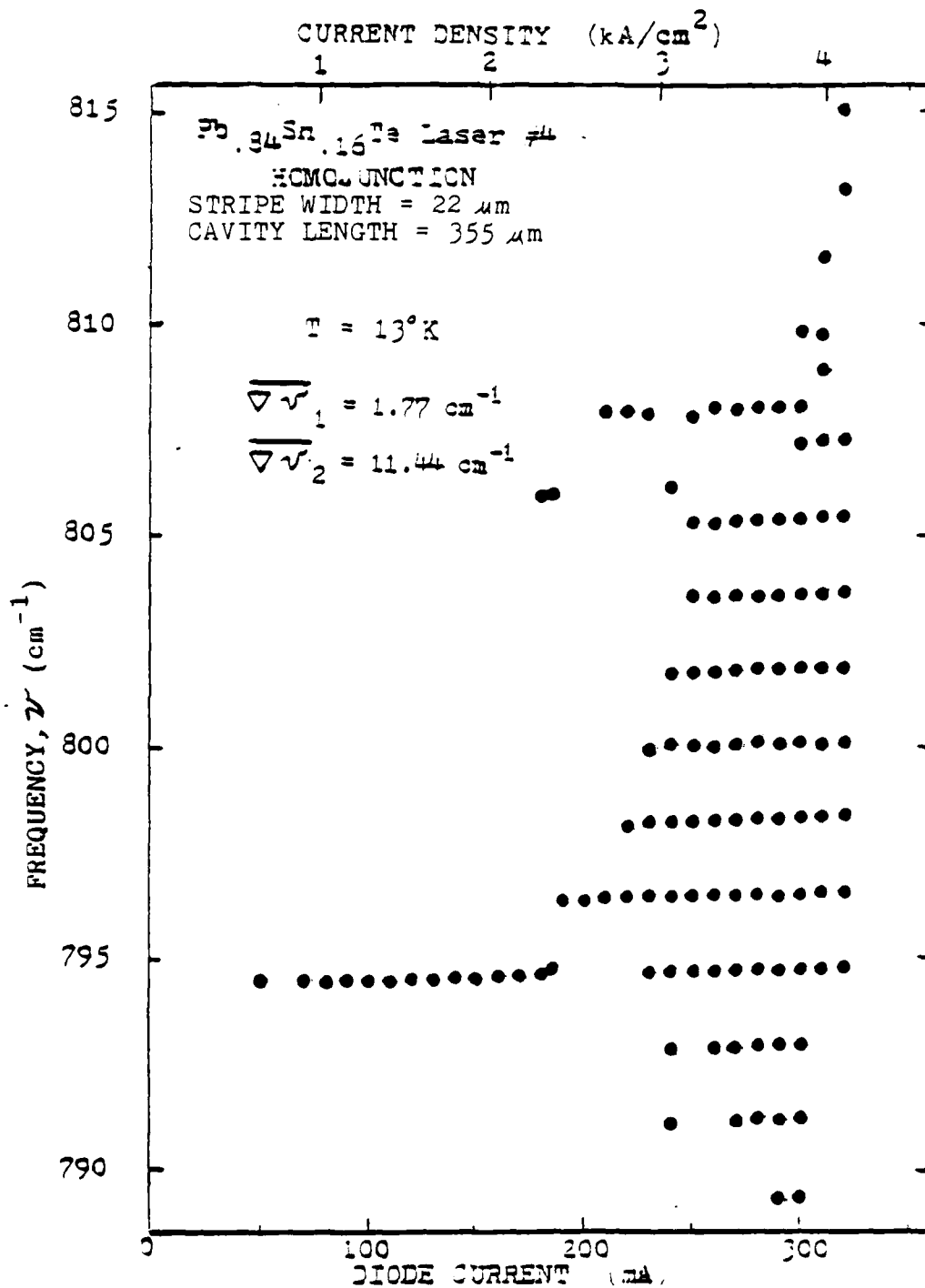
FIGURE 19   FREQUENCY vs. DIODE CURRENT for Laser Diode No. 4

RELATIVE OUTPUT POWER vs. MAGNETIC FIELD

THRESHOLD CURRENT vs. MAGNETIC FIELD

Figure 20. Output Power and Threshold vs. Magnetic Field
for Laser Diode No. 4
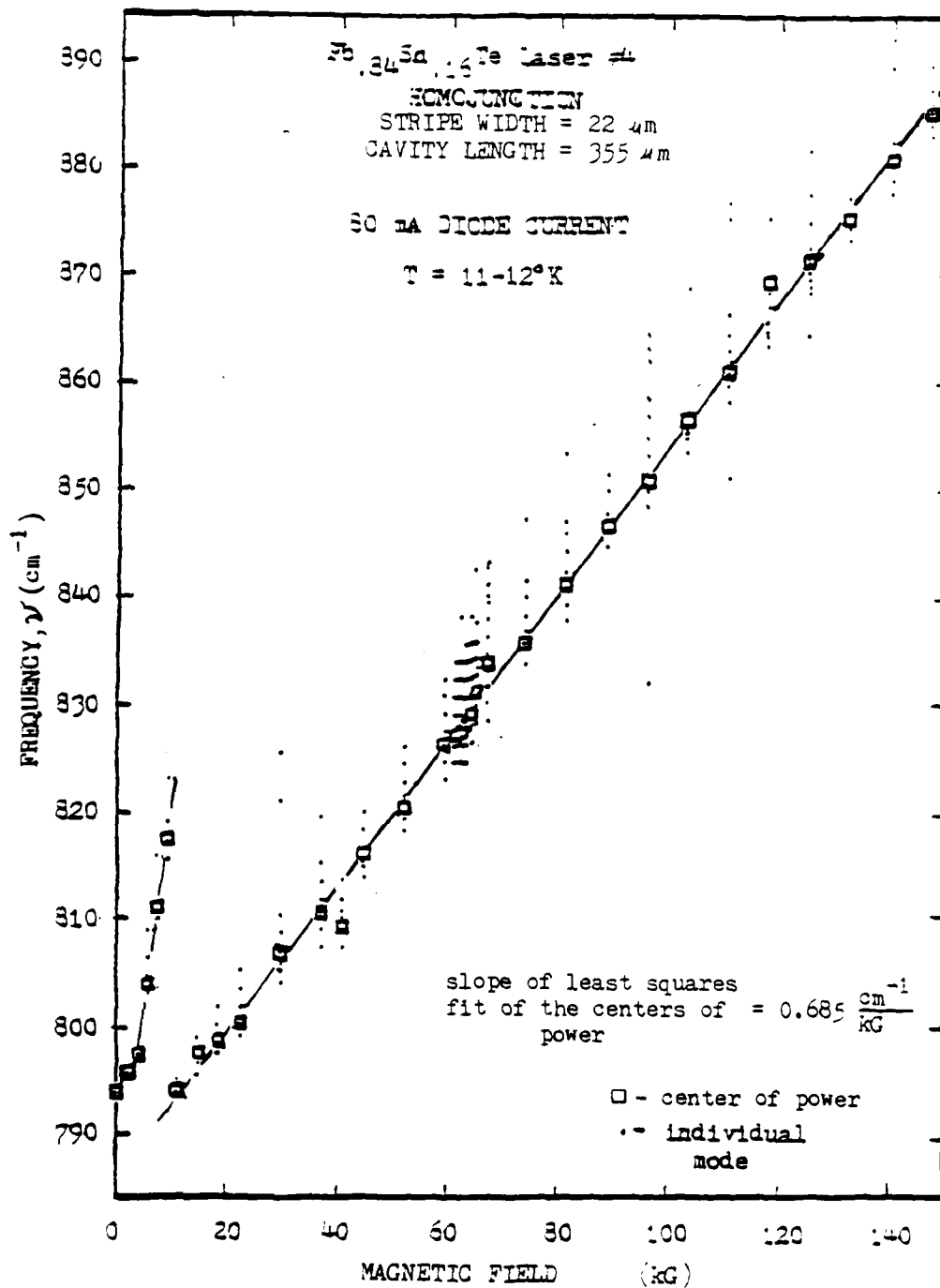
FIGURE 21.   FREQUENCY vs. MAGNETIC FIELD for Laser Diode No. 4

2. Laser Diode No. 2

Laser diode No. 2 is a double heterostructure stripe-configured laser diode. It has a $Pb_{.86}Sn_{.14}Te$ active region with confinement layers of $(Pb_{.86}Sn_{.14})_{.97}Yb_{.03}Te$. The stripe width is approximately 25 μm and the active region is 1.5 μm thick. The cavity length is not known. The plot of frequency versus diode current for diode No. 2 is shown in Figure 22. The separation between modes was so varied that an average repeated separation was not computed.

This diode did not operate very well at high magnetic field. There was an initial sharp rise of power with magnetic field but by 15 kG the laser output was greatly reduced as seen in the relative output power versus magnetic field plot (upper half of Figure 23). The frequency versus magnetic field plot, shown in Figure 24, also reflects this drop in power. Even at 300 mA of diode current I was unable to get a spectrum at magnetic field strengths greater than 15 kG.
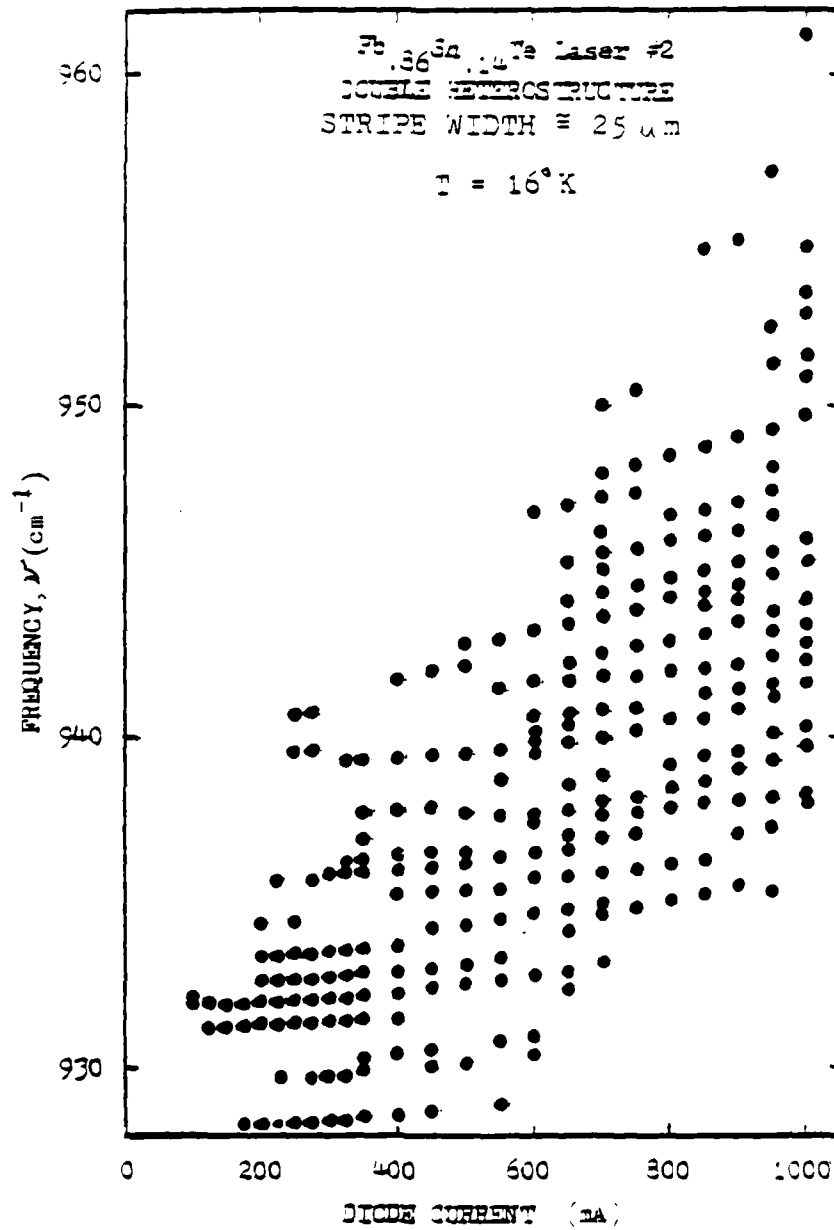
FIGURE 22   FREQUENCY vs. DIODE CURRENT for Laser
Diode No. 2

RELATIVE OUTPUT POWER vs. MAGNETIC FIELD
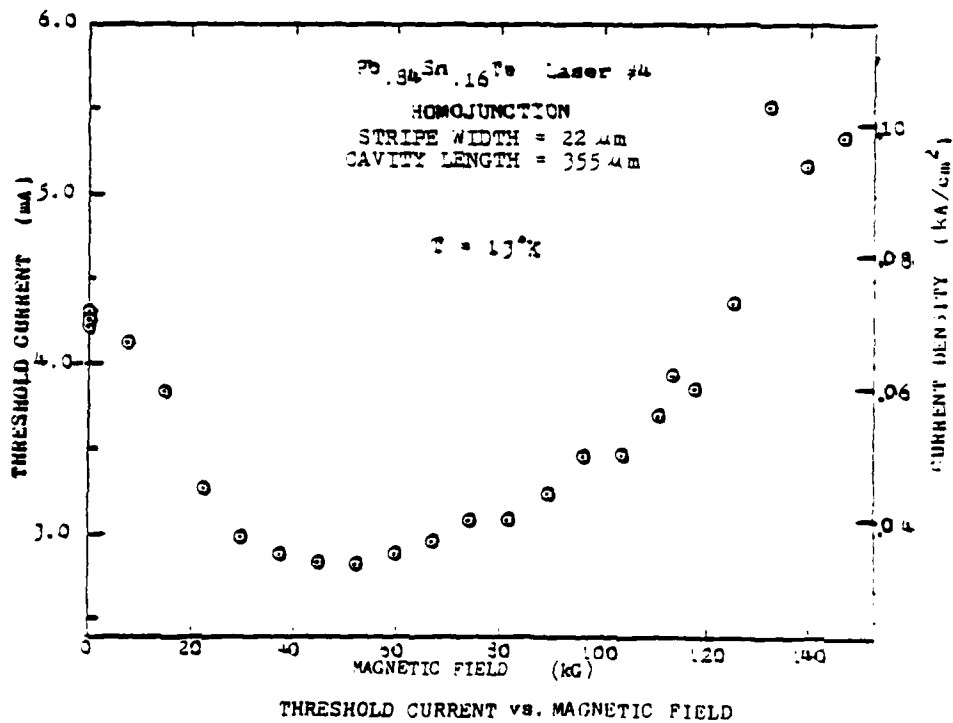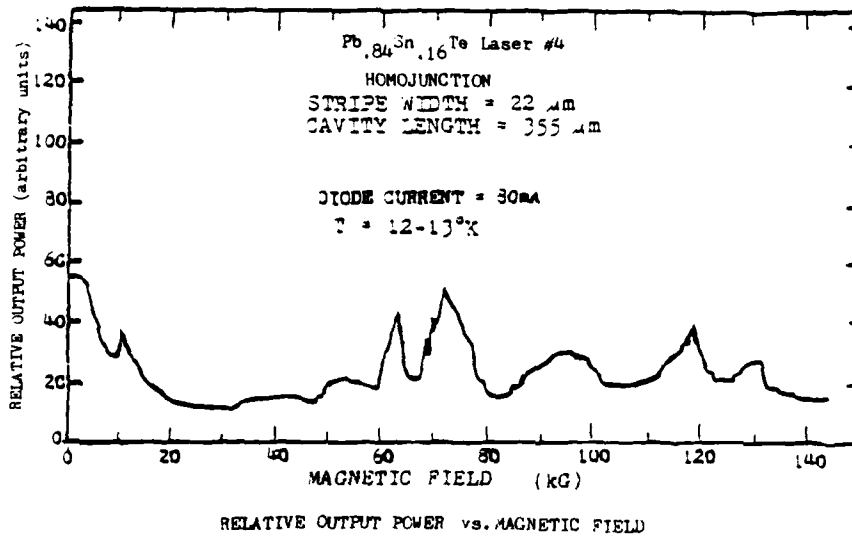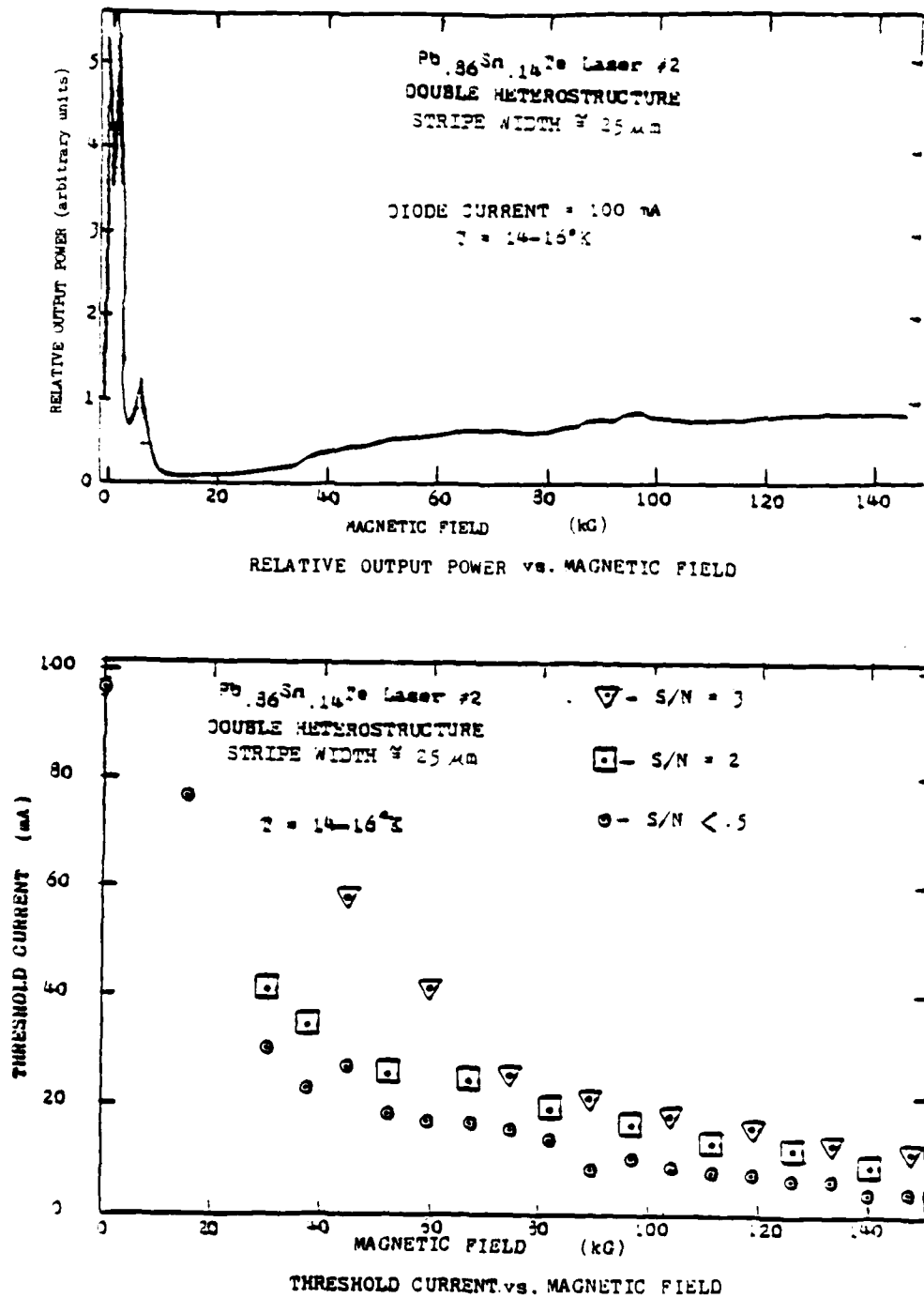

THRESHOLD CURRENT vs. MAGNETIC FIELD

Figure 23. Output Power and Threshold vs. Magnetic Field
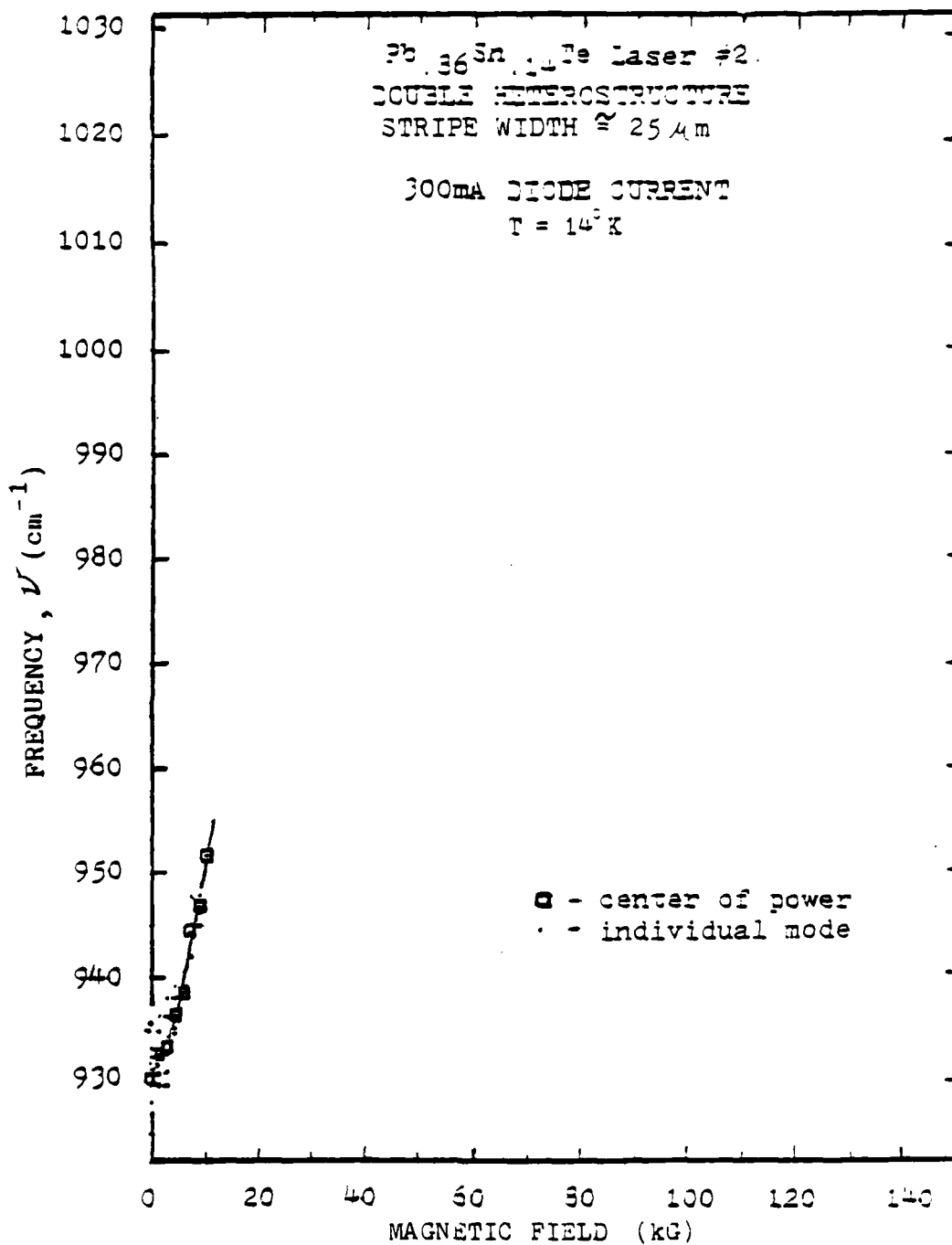for Laser Diode No. 2

FIGURE 24.   FREQUENCY vs. MAGNETIC FIELD for Laser
Diode No. 2

3. Laser Diode No. 5

Laser diode No. 5 is a 300 $\overset{o}{A}$ quantum well laser with an active region of PbTe. The confinement layers are composed of $Pb_{1-x}Eu_xSe_yTe_{1-y}$ with x = .018 at the boundaries with the active region. The value of y was adjusted as necessary for lattice matching and is roughly equal to x [9]. The complete barrier structure is in Appendix D. The stripe width is 16 μm and the cavity length equals 323 μm for a stripe surface area of $5.17x10^{-5}cm^2$. The plots of Figures 25 and 26 are frequency versus diode current plots for laser diode No. 5. Figure 25 is from data taken while the thermistor, attached to the laser heat sink, registered a temperature of $11^{o}K$. The thermistor temperature ranged from 81° to $82^{o}K$ when taking data for Figure 26. The data at $11^{o}K$ (Figure 25) revealed two average separations. The smaller one, $\overline{\nabla\nu}_1$, equaled 4.92 cm^{-1} and the larger one, $\overline{\nabla\nu}_2$, equaled 12.50 cm^{-1}. The data at 81° to 82° (Figure 26) showed two large separations at 65.21 cm^{-1} and 150.44 cm^{-1}.

The relative output power versus magnetic field plot in the upper half of Figure 27 was taken at 80 mA of diode

---

[9] as per conversations with Dr. Dale Partin, General Motors Research Laboratories.

current. The threshold current versus magnetic field was measured both with liquid helium in the cold finger (lower half Figure 27) and with liquid nitrogen in the cold finger (Figure 28). Figure 29 is a plot of the frequency versus magnetic field strength at 80 mA diode current. The slope of the lower line was 1.77 cm^{-1}/kG as indicated.

FIGURE 25 FREQUENCY vs. DIODE CURRENT for Laser
Diode No. 5

FIGURE 26 FREQUENCY vs. DIODE CURRENT for Laser
Diode No. 5

RELATIVE OUTPUT POWER vs. MAGNETIC FIELD

THRESHOLD CURRENT vs. MAGNETIC FIELD

Figure 27. Output Power and Threshold vs. Magnetic Field
for Laser Diode No. 5

49

THRESHOLD CURRENT vs. MAGNETIC FIELD

Figure 28. Threshold Current vs. Magnetic Field
for Laser Diode No. 5

Figure 29. Frequency vs. Magnetic Field for Laser Diode No. 5

4. Laser Diode No. 6

Laser diode No. 6 is a 600 Å quantum well laser. It has an active region composed of PbTe and $Pb_{1-x}Eu_xSe_yTe_{1-y}$ confinement layers with x = .019 at the boundaries with the active region. As with laser diode No. 5 the complete confinement structure is shown in Appendix D. This stripe-configured laser diode has a stripe width of 23 μm and a cavity length of 317 μm for a stripe surface area of 7.27×10^{-5} cm^2. Figures 30 and 31 are the frequency versus diode current plots for laser diode No. 6 at $9°K$ and $81°K$ respectively. No average mode separation was clearly identifiable.

The relative output power versus magnetic field plot in the upper half of Figure 32 shows behavior similar to diode No. 2 in that it was high initially and then dropped a great deal by a magnetic field strength of 15 kG. The threshold pattern (lower half of Figure 32) for this laser was completely different from the other lasers measured. It rose then fell where the others generally fell then (except for diode No. 2) rose again. By driving the diode with 300 mA of diode current I was able to produce a reasonable frequency versus magnetic field strength plot as seen in Figure 33. The few centers of power shown yielded a slope of 1.95 cm^{-1}/kG as indicated.
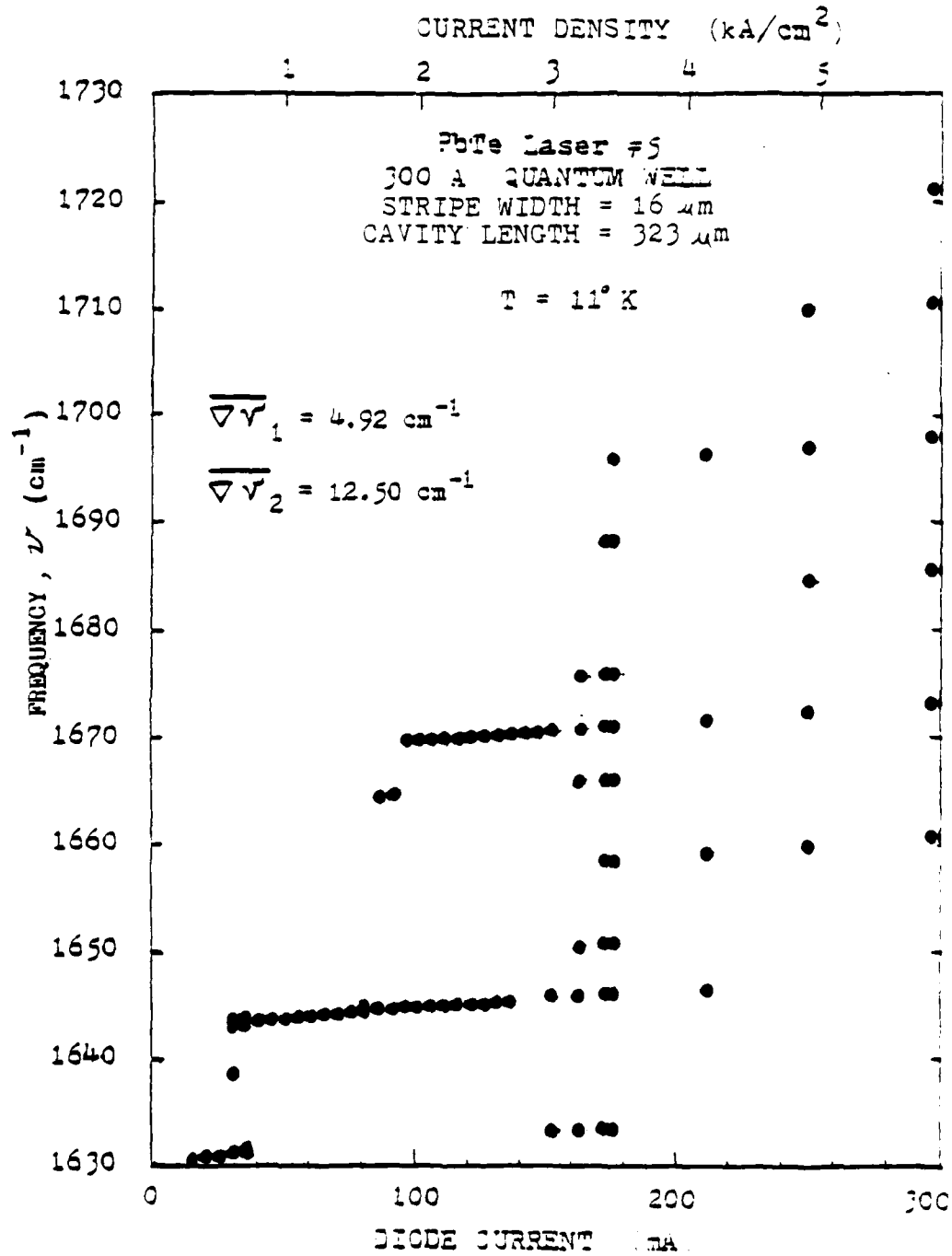
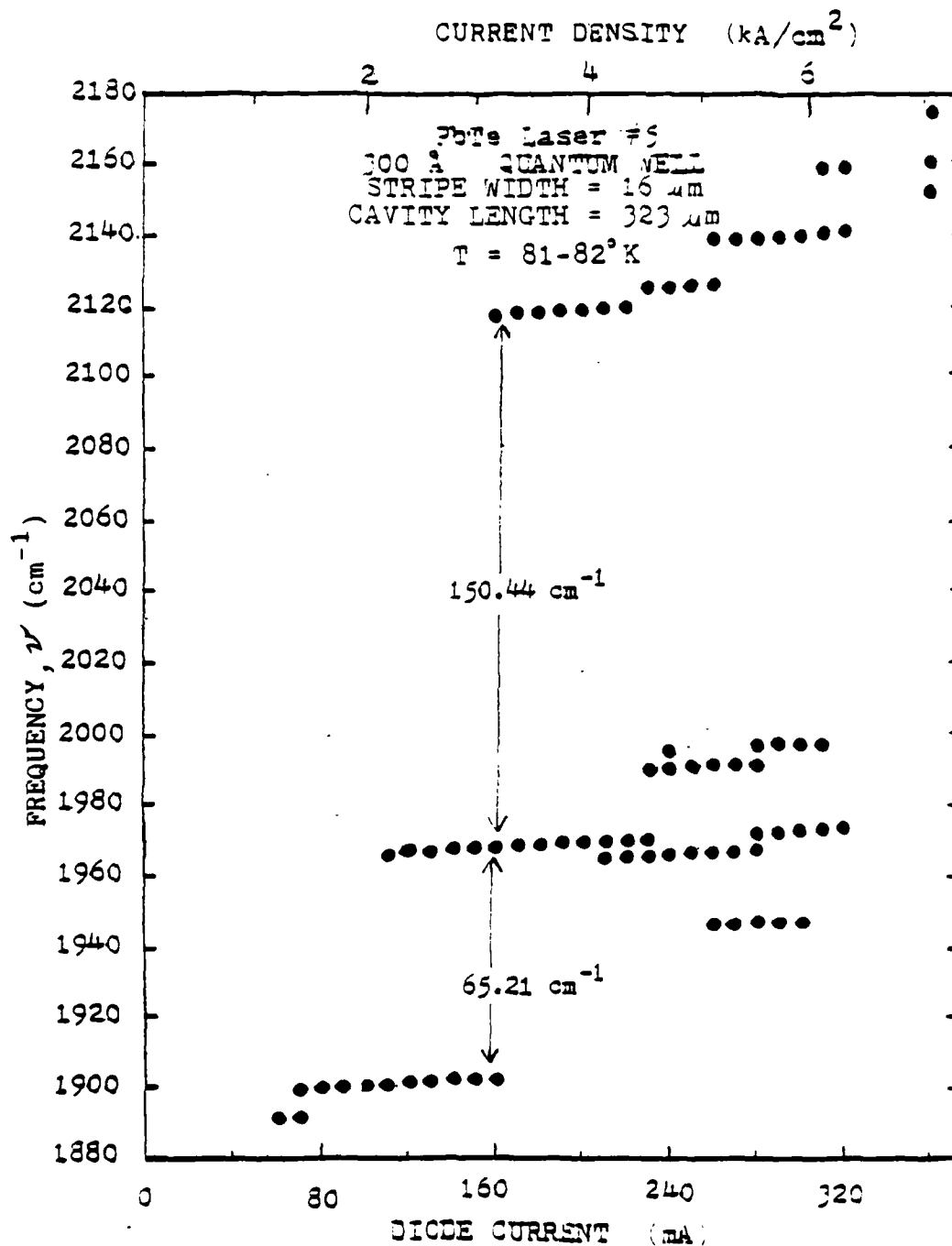FIGURE 30.   FREQUENCY vs. DIODE CURRENT for Laser Diode No. 6

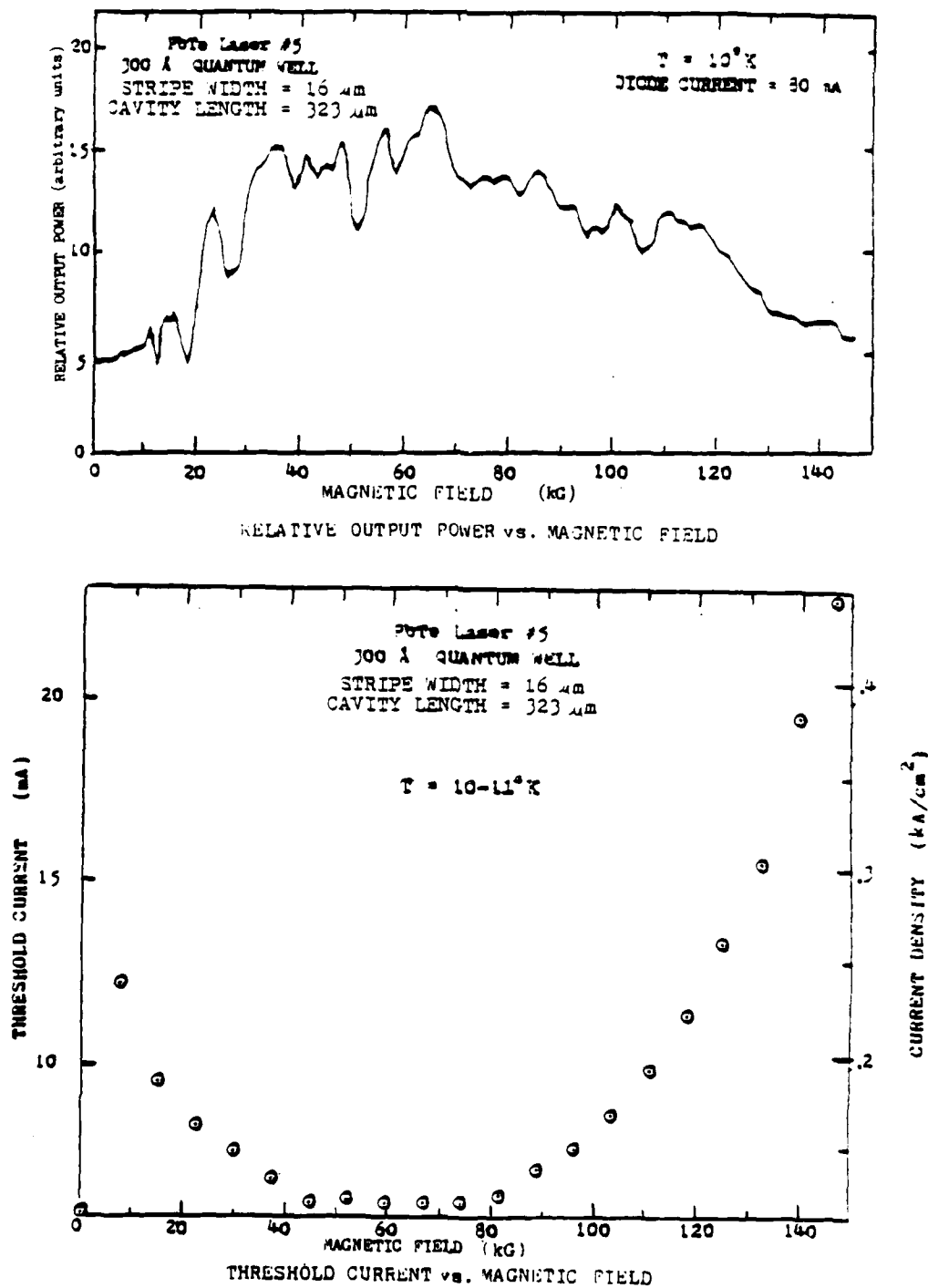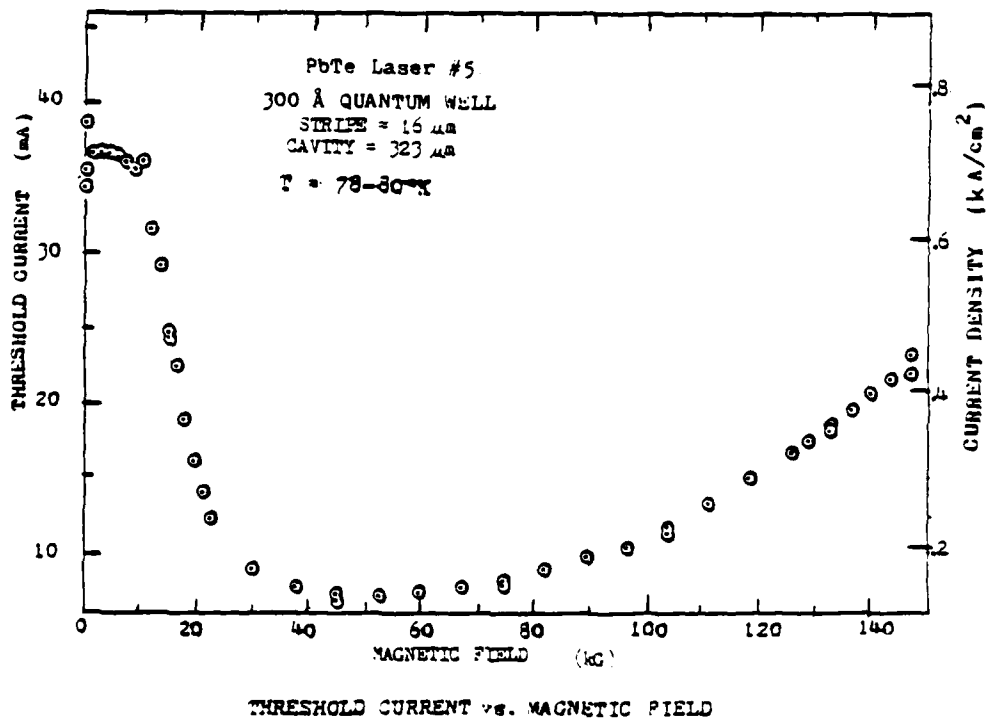FIGURE 31.   FREQUENCY vs. DIODE CURRENT for Laser
Diode No. 6
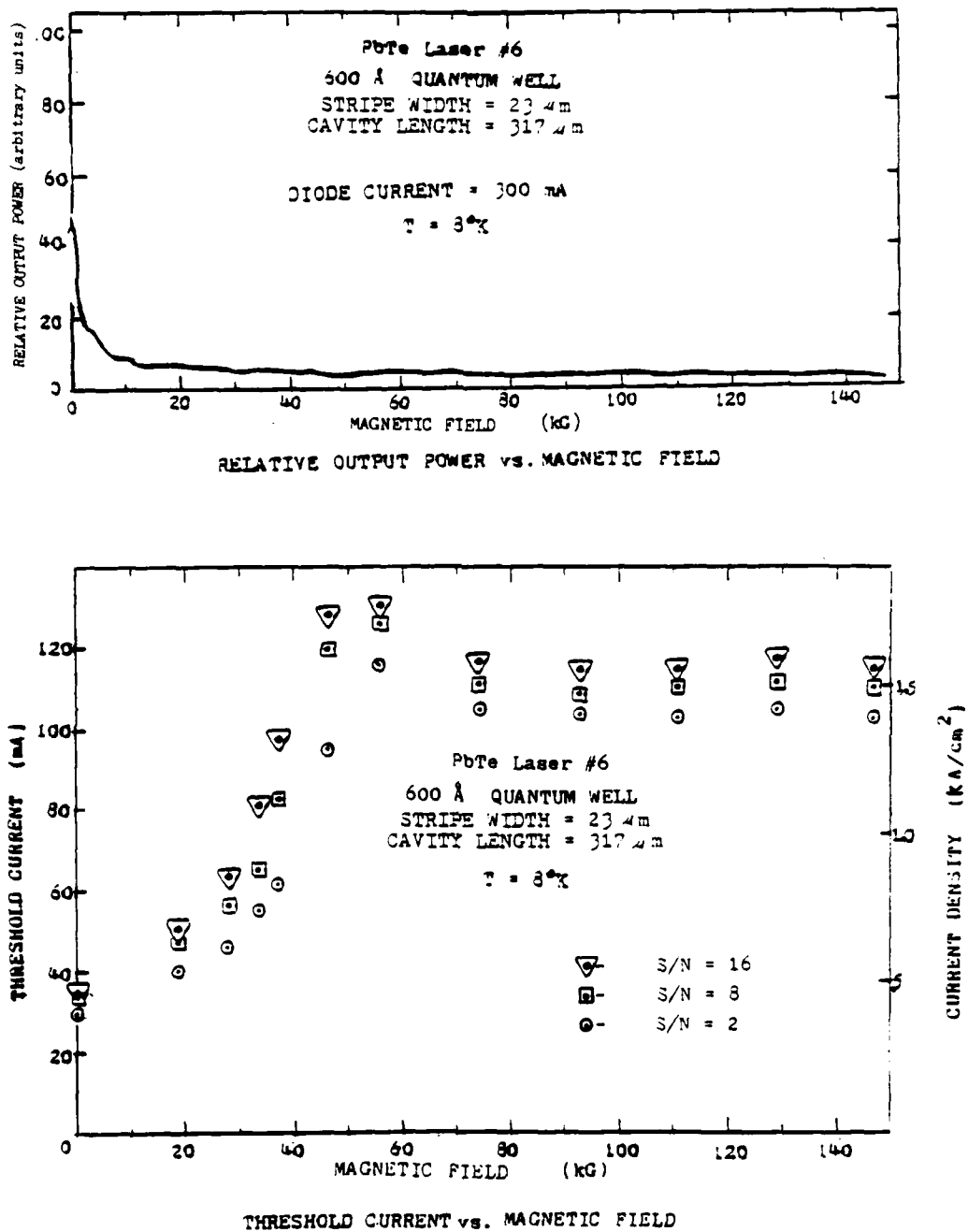
Figure 32. Output Power and Threshold vs. Magnetic Field
for Laser Diode No. 6

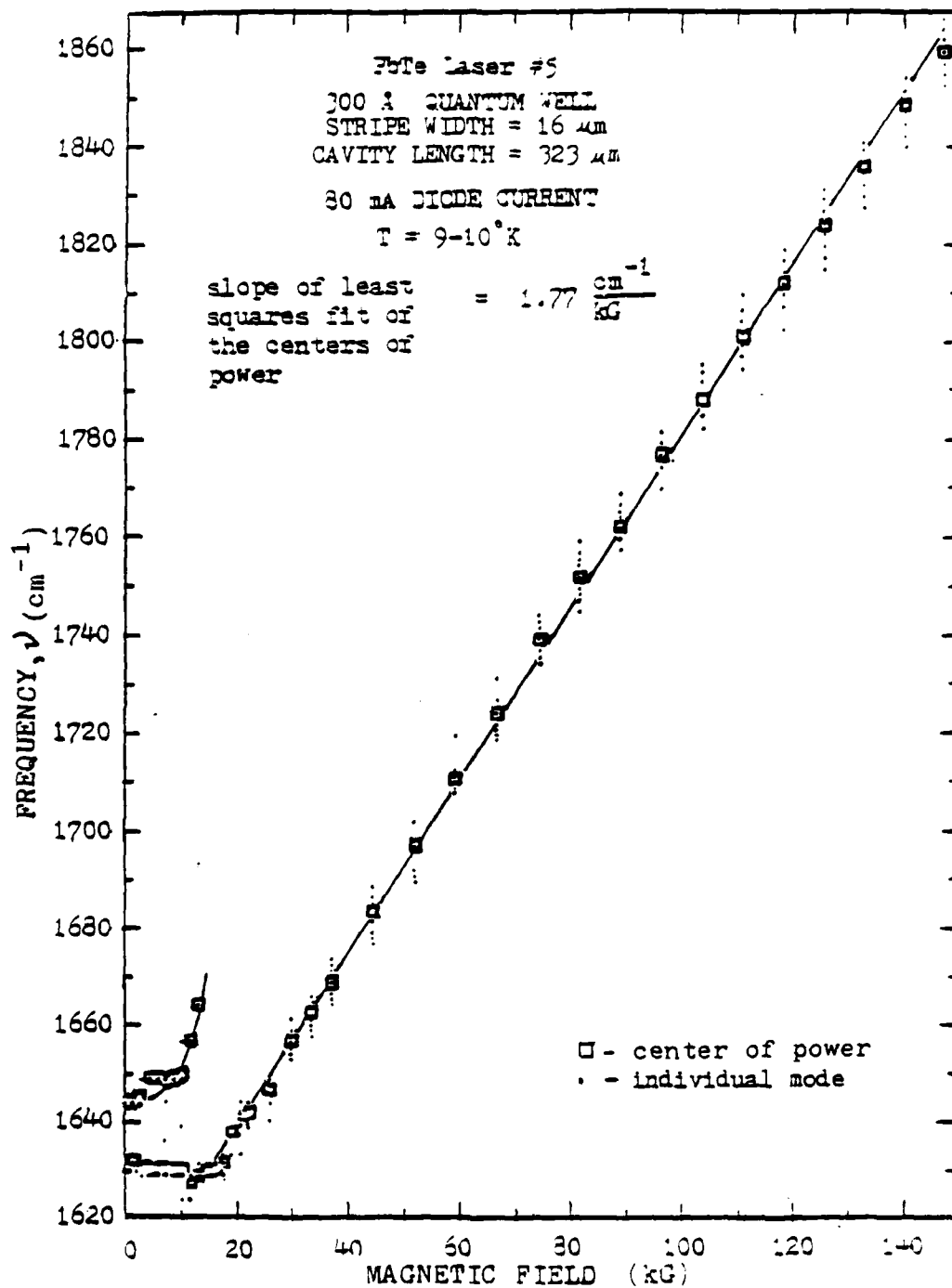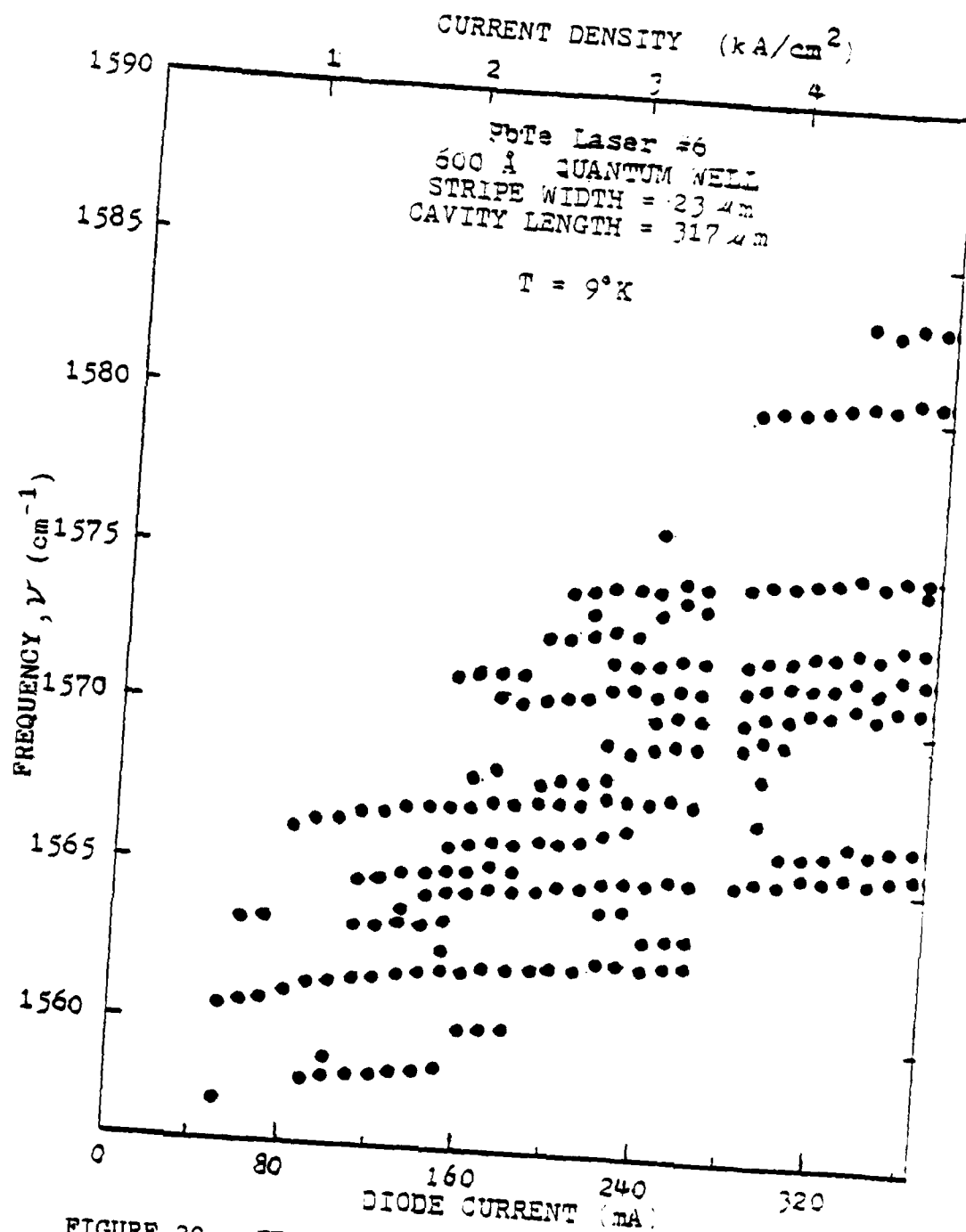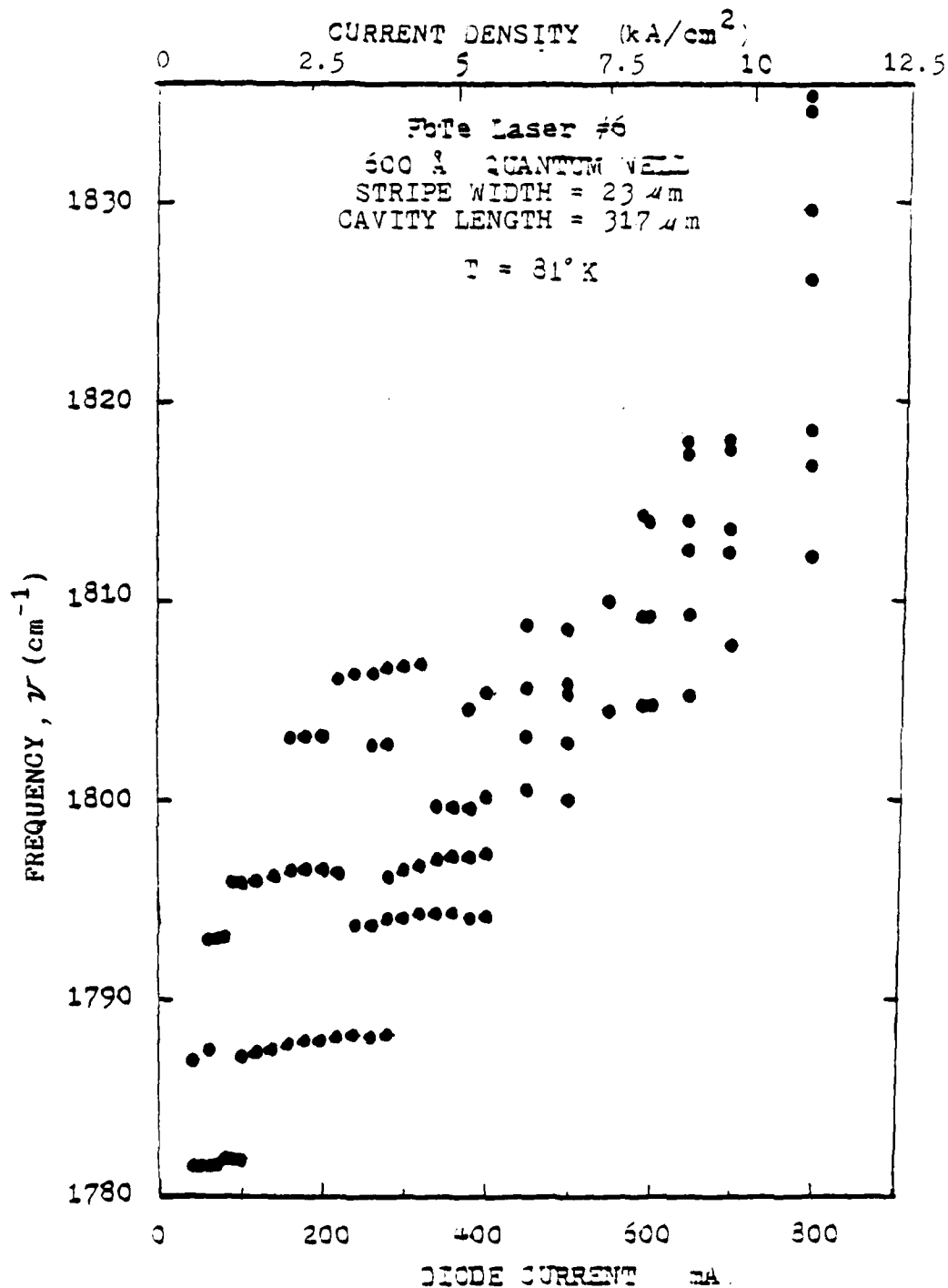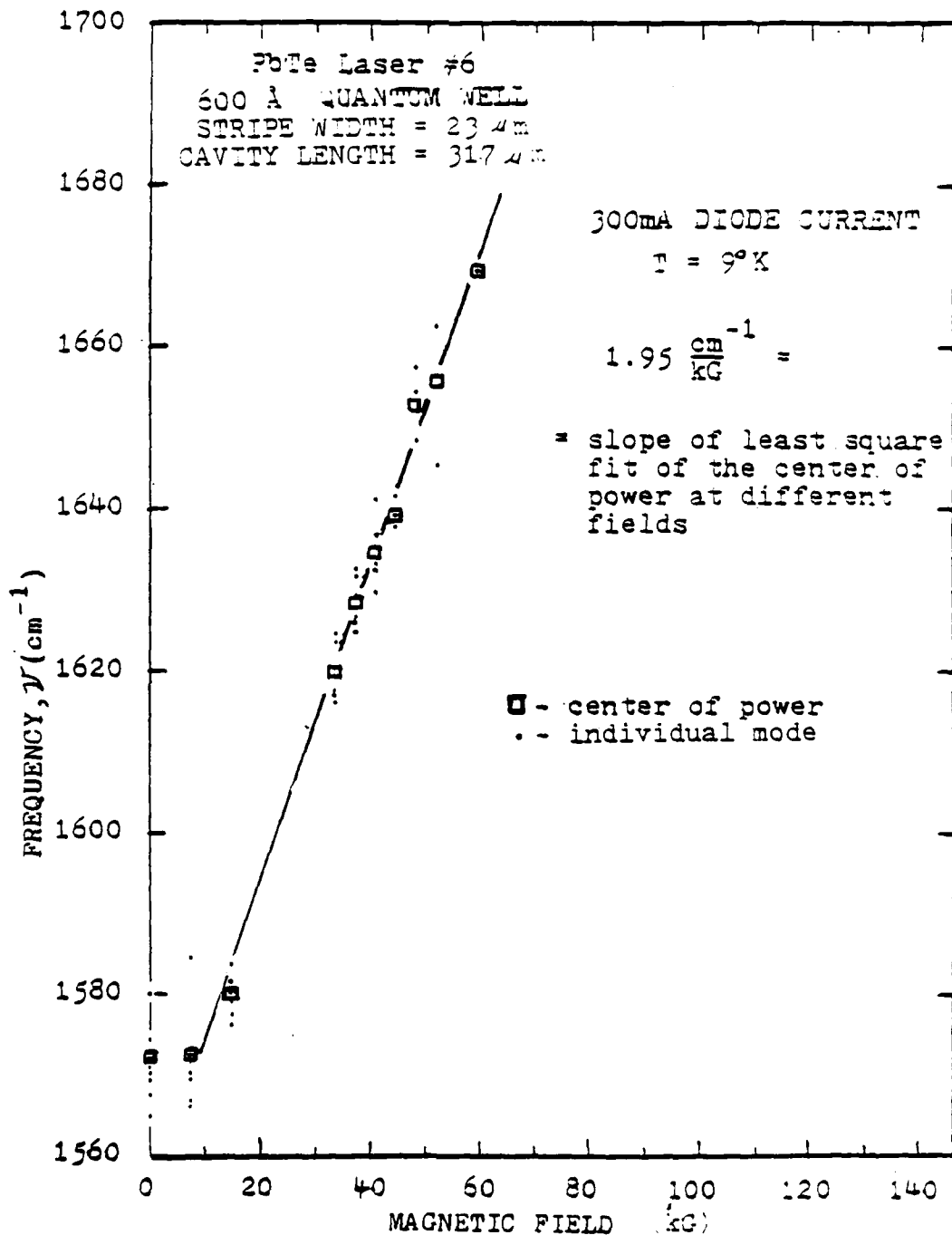FIGURE 33. FREQUENCY vs. MAGNETIC FIELD for Laser Diode No. 6

IV. DATA INTERPRETATION

As mentioned in the Introduction, the primary purpose of
this thesis is to present the experimental procedures and
results. In view of time limitation, I will not attempt to
explain all the data taken during the course of this thesis.
I will focus on one interesting feature observed for the 300 $\overset{\circ}{A}$
quantum well laser (Diode No. 5) viz. the large separations
between laser frequencies. In this section I will consider
a simple model of an electron in a potential well to determine
the quantum mechanical energy levels in the well in order to
account for these large frequency separations. I will start
by assuming the energy bands are parabolic and then include
corrections for the nonparabolicity after outlining the solu-
tion to the simpler model. The theory will then be compared
to the results shown in Figure 26. I will conclude the sec-
tion with a few short comments on the interpretation of some
of the other data presented.

Figure 34 shows the stripe mesa of a quantum well laser
like laser diode No. 5 or No. 6. The figure is not to scale
since the actual thickness of the quantum well (represented by
the cross-hatched region), 2a, is more than 300 times smaller
than the stripe width, b, for the lasers used in this experi-
ment. The coordinate system shown in the figure is centered
in the middle of the quantum well on the edge of the stripe
mesa. For diode No. 5 the material above and below the quan-
tum well is $Pb_{.98}Eu_{.02}Se_yTe_{1-y}$ (see Appendix D, Figure D1).
The well itself is PbTe. $Pb_{.98}Eu_{.02}Se_yTe_{1-y}$ has an energy
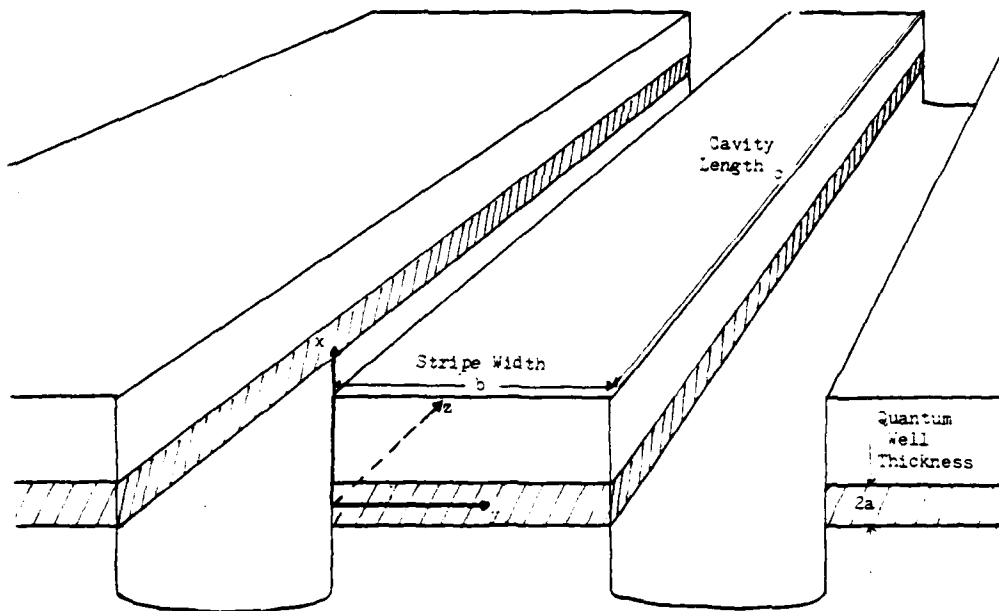
Figure 34.   The stripe-mesa quantum well laser with
             coordinate system and cavity dimensions.

band gap, Eg', that is 99 meV larger than the energy band gap, Eg, of PbTe.[10] This difference in energy gap, ΔEg, between the two materials forms two potential wells of depth V_c and V_v as shown in Figure 35 so that

$$\Delta Eg = V_c + V_v = 99 \text{ meV} \tag{1}$$

The x direction in Figures 34 and 35 corresponds to the <100> crystal axis. However, in PbTe the constant energy surfaces are four elongated ellipsoids along the <111> crystal directions.[11] The Hamiltonian, H', for these constant energy ellipsoids is

$$H' = \frac{P_x^{2'} + P_y^{2'}}{2m_t} + \frac{P_z^{2'}}{2m_\ell} + V \tag{2}$$

when z' axis is aligned along the <111> crystal axis. The m_ℓ and m_t are the longitudinal (along the <111> axis) and the transverse (perpendicular to the <111> axis) effective masses, respectively. To apply the above Hamiltonian to the quantum well problem, the coordinate system must be changed from the primed coordinates with the z' axis along the <111> crystal axis to the unprimed coordinates with the x axis along the <100> crystal axis. Figure 36 shows one of the four constant energy ellipsoids along the <111> crystal axis (z' axis) and the primed and unprimed coordinate systems. The cosine of the

---

[10]From conversations with Dr. Dale Partin. He determined Eg' from lasers with $Pb_{1-x}Eu_xSe_yTe_{1-4}$ active regions.

[11]Tsidilkovski, I.M., _Band Structure of Semiconductors_ © 1982 Pergamon Press Ltd., p. 176.
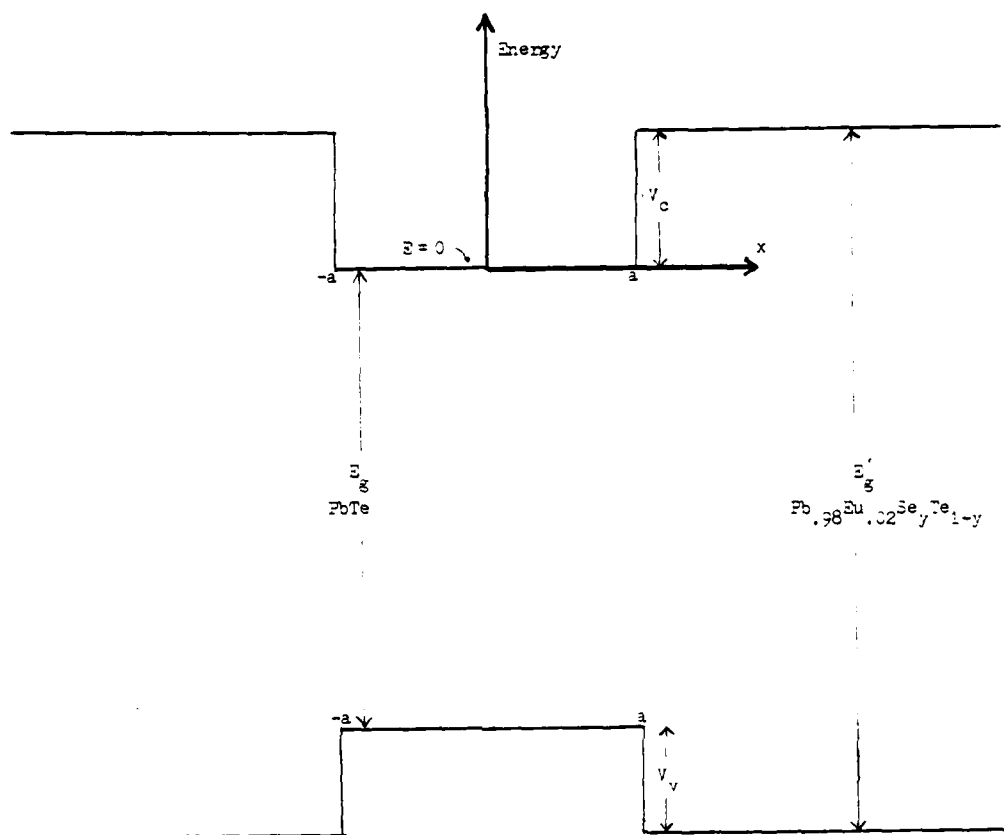
Figure 35.   The potential well structure.
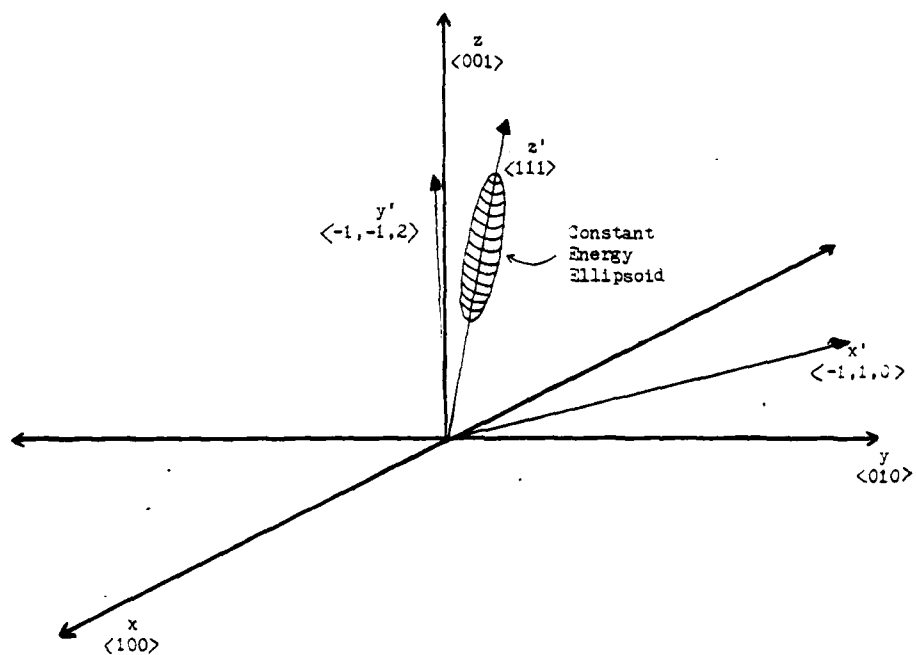
Figure 36. One of the four constant energy ellipsoids
and each of the primed and unprimed coordinates
with its corresponding crystal axis.

angle between a primed and an umprimed coordinate direction is the dot product of the associated unit vectors along those directions,

$$\cos\theta_{aa'} = \hat{a} \cdot \hat{a}' = \frac{\bar{a}}{|\bar{a}|} \cdot \frac{\bar{a}'}{|\bar{a}'|} \tag{3}$$

Thus

$$\cos\theta_{xx'} = \frac{(1,0,0)}{|(1,0,0)|} \cdot \frac{(-1,1,0)}{|(-1,1,0)|} = -\frac{1}{\sqrt{2}} \tag{4}$$

$$\cos\theta_{yx'} = \frac{(0,1,0)}{|(0,1,0)|} \cdot \frac{(-1,1,0)}{|(-1,1,0)|} = +\frac{1}{\sqrt{2}} \tag{5}$$

$$\cos\theta_{zx'} = \frac{(0,0,1)}{|(0,0,1)|} \cdot \frac{(-1,1,0)}{|(-1,1,0)|} = 0 \tag{6}$$

So that the momentum in the x'-direction, P_x', is given by

$$P_x' = -\frac{1}{\sqrt{2}} P_x + \frac{1}{\sqrt{2}} P_y \tag{7}$$

or

$$P_x' = \frac{1}{\sqrt{2}} (P_y - P_x) \tag{8}$$

Similarly

$$P_y' = \frac{1}{\sqrt{6}} (-P_x - P_y + 2P_x) \tag{9}$$

$$P_z' = \frac{1}{\sqrt{3}} (P_x + P_y + P_z) \tag{10}$$

Using equations (8), (9) and (10) equation (2) may be written
as

$$H = (\frac{P_x^2}{2} + \frac{P_y^2}{2} + \frac{P_x^2}{2})(\frac{2}{3}\frac{1}{m_t} + \frac{1}{3}\frac{1}{m_\ell})$$

$$- (\frac{P_x P_z}{2} + \frac{P_x P_z}{2} + \frac{P_x P_y}{2})(\frac{2}{3}\frac{1}{m_t} - \frac{2}{3}\frac{1}{m_\ell}) + V \qquad (11)$$

which is the Hamiltonian, H, in the unprimed coordinate sys-
tem. Within the diode the potential, V, is assumed to be only
a function of x. Therefore, the momentum distributions in the
y and z directions for a large group of electrons or holes
should be symmetric about zero. If an average is taken over
all the momenta, then the terms in equation (11) which are
not squared should average to zero leaving,

$$H = (\frac{P_x^2}{2} + \frac{P_y^2}{2} + \frac{P_z^2}{2})(\frac{2}{3}\frac{1}{m_t} + \frac{1}{3}\frac{1}{m_\ell}) \qquad (12)$$

Thus the effective mass, m*, can be defined as

$$\frac{1}{m^*} = (\frac{2}{3}\frac{1}{m_t} + \frac{1}{3}\frac{1}{m_\ell}) \qquad (13)$$

such that H takes on the standard form of

$$H = \frac{P_x^2}{2m^*} + \frac{P_y^2}{2m^*} + \frac{P_z^2}{2m^*} + V(x) \qquad (14)$$

If the zero of energy is considered to correspond to the
bottom of the PbTe conduction band (see Figure 35) then for

the conduction band

$$V(x) = 0 \qquad \text{for} \qquad |x| < a \qquad\qquad (15)$$

$$V(x) = V_c \qquad \text{for} \qquad |x| > a \qquad\qquad (16)$$

and for the valence band

$$V(x) = -E_g \qquad \text{for} \qquad |x| < a \qquad\qquad (17)$$

$$V(x) = -E_g - V_v \qquad \text{for} \qquad |x| > a \qquad\qquad (18)$$

where E_g refers to the energy gap of PbTe. The Schrondinger equations for the conduction band are

$$-\frac{\hbar^2}{2m_c^*} \nabla^2 \psi = E\psi \qquad \text{for} \qquad |x| < a \qquad\qquad (19)$$

and

$$\frac{\hbar^2}{2m_c^{*\prime}} \nabla^2 \psi' + V_c \psi' = \cdot E\psi' \qquad \text{for} \qquad |x| > a \qquad\qquad (20)$$

where m_c^* and $m_c^{*\prime}$ are the conduction band effective masses in PbTe and $Pb_{.98}Eu_{.02}Se_yTe_{1-y}$ respectively. The relationship between m^* and $m^{*\prime}$ (valence or conduction) is given by[12]

$$m^{*\prime} = \frac{E_g}{E_g} m^* \qquad\qquad (21)$$

_____

[12] This assumes $m^* = \frac{E_g m}{P^2}$ and $\frac{m}{P^2} = $ constant in PbTe and $Pb_{.98}Eu_{.02}Se_yTe_{1-y}$.

Equations (19) and (20) can be separated into equations for x, y, and z. The solutions to the y and z equations with infinite potential barriers at the cavity walls are plain waves with nearly continuous (relative to E_x, since a b or c) energies

$$E_{yr} = \frac{\hbar^2}{2m^*} \frac{r^2 \pi^2}{b^2} \quad \text{for} \quad 0<y<b \quad \text{and} \quad r = 1,2,3 \ldots \quad (22)$$

$$E_{zq} = \frac{\hbar^2}{2m^*} \frac{q^2 \pi^2}{c^2} \quad \text{for} \quad 0<z<c \quad \text{and} \quad q = 1,2,3 \ldots \quad (23)$$

So that the remaining x equations are

$$\frac{\partial^2}{\partial x^2} g(x) + (\frac{2m_c^*}{\hbar^2} E_c + \frac{r^2 \pi^2}{b^2} + \frac{q^2 \pi^2}{c^2}) g(x) = 0 \quad \text{for} \quad |x|<a \quad (24)$$

$$\frac{\partial^2}{\partial x^2} g'(x) - [\frac{2m_c^*}{\hbar^2} \frac{E_{g'}}{E_g} (V_c - E_c) - \frac{r^2 \pi^2}{b^2} - \frac{q^2 \pi^2}{c^2}] g'(x) = 0$$

$$\text{for} \quad |x|>a \quad (25)$$

where

$$\psi(x,y,z) = g(x) h(y) j(z) \quad (26)$$

Now if ε_c, k_c and k_c' are defined as

$$\varepsilon_c = E_c + \frac{\hbar^2}{2m^*} (\frac{r^2 \pi^2}{b^2} + \frac{q^2 \pi^2}{c^2}) \quad (27)$$

$$k_c = \sqrt{\frac{2m_c^*}{\hbar^2} \varepsilon_c} \quad (28)$$

$$k_c' = \sqrt{\frac{2m^*c}{\hbar^2} \frac{E_g'}{E_g} (V_c - \varepsilon_c)} \qquad (29)$$

then equations (24) and (25) become

$$\frac{\partial^2 g}{\partial x^2} + k_c^2 g = 0 \qquad (30)$$

$$\frac{\partial^2 g'}{\partial x^2} - k_c'^2 g' = 0 \qquad (31)$$

Solving equations (30) and (31) and matching g(x) and g(x)' at x = ±a yields

$$k_c' = k_c \tan k_c a \qquad (32)$$

or

$$k_c' = -k_c \cot k_c a \qquad (33)$$

which are transcendental equations. The valence band calculations yielded the same equations if k_c and k_c' are replaced by

$$k_v = \sqrt{\frac{2m^*_v}{\hbar^2} \varepsilon_v} \qquad (34)$$

$$k_v' = \sqrt{\frac{2m^*_v}{\hbar^2} \frac{E_g'}{E_g} (V_v - \varepsilon_v)} \qquad (35)$$

respectively and where

$$\varepsilon_v = \left[|E_v| + \left(\frac{r^2 \pi^2}{b^2} + \frac{q^2 \pi^2}{c^2} \right) \frac{\hbar^2}{2m^*_v} \right] - E_g \qquad (36)$$

and m^*_v is the absolute value of the hole effective mass in PbTe. Solutions to equations (32) and (33) can be found graphically or numerically. To graphically solve the equations, first find k' in terms of k as

$$k' = \sqrt{\frac{E_g'}{E_g} \left(\frac{2m_*}{\hbar^2} V - k^2 \right)} \tag{37}$$

where the references to valence or conduction band have been dropped since the equations have the same form. Substituting equation (37) into (32) and (33) and dividing by k yields

$$\sqrt{\frac{E_g'}{E_g} \left(\frac{2m^*V}{\hbar^2 k^2} - 1 \right)} = \tan(ka) \tag{38}$$

$$\sqrt{\frac{E_g'}{E_g} \left(\frac{2m^*V}{\hbar^2 k^2} - 1 \right)} = -\cot(ka) \tag{39}$$

By plotting both sides of equations (38) and (39) as functions of k the solutions k_1 and k_2 can be found as shown in Figure 37. The square root in equations (38) and (39) becomes imaginary at k values greater than

$$k = \sqrt{\frac{2m^*V}{\hbar^2}} \tag{40}$$

and this is the $k_{cut\ off}$ value shown in the figure.

The values of k_1 and k_2 are the allowed values of k from which the energy levels in the well can be computed using the
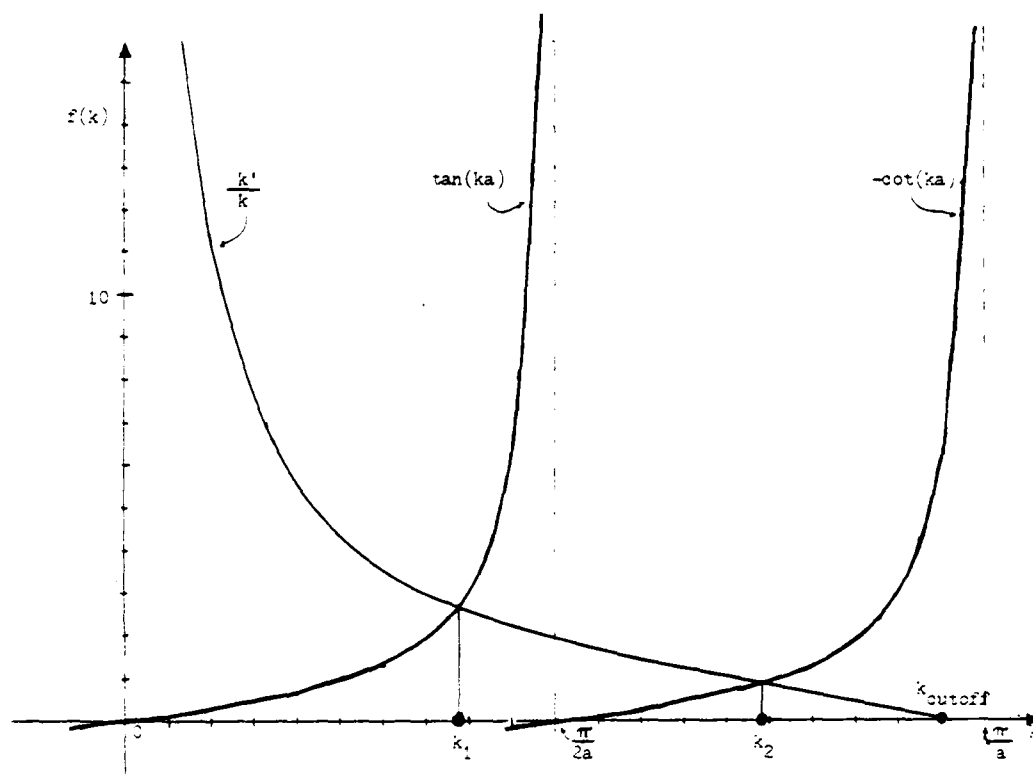
Figure 37.   The graphical solutions of quantum well
transcendental equations (38) and (39).

appropriate definition for k. Therefore

$$\varepsilon_{n_{c,v}} = \frac{k_n^2 \hbar^2}{2m^*_{c,v}} \tag{41}$$

where $\varepsilon_{n_{c,v}}$ is defined by equations (27) or (36) and k_n is either k_1 or k_2, the solution to the transcendental equations (38) or (39).

Up to this point two assumptions have been made, first that the constant energy surfaces are ellipsoids and second that the bands are parabolic. These assumptions allowed the presentation of the problem in a simple manner. Now that the problem has been presented, corrections can be made. The distortions in the ellipsoid, although present, are small and can be neglected.[13]

The nonparabolicity of the band, however, should be included. Using the Kane model this can be done by replacing the longitudinal and transverse masses with energy dependent masses[14]

$$m_\ell(\varepsilon) = m_{\ell o}(1 + \frac{2\varepsilon}{E_g}) \tag{42}$$

$$m_t(\varepsilon) = m_{to}(1 + \frac{2\varepsilon}{E_g}) \tag{43}$$

Placing equations (42) and (43) in equation (13) we find that

---

[13] G.M.T. Foley and D.N. Langenberg, Phys. Rev. B., Vol. 15, No. 10, p. 4850-67, May 1977.

[14] I.M. Tsidilkovski, p. 182.

$$m^*(\varepsilon) = m_o^* \left(1 + \frac{2\varepsilon}{E_g}\right) \tag{44}$$

and

$$m^{*\prime}(\varepsilon) = \frac{E_g{}'}{E_g} m_o^* \left(1 + \frac{2\varepsilon}{E_g{}'}\right) \tag{45}$$

These new definitions of the effective masses are inserted into the definitions of $k_{c,v}$ and $k'_{c,v}$ to yield

$$k = \sqrt{\frac{2m_o^*}{\hbar^2} \left(1 + \frac{2\varepsilon}{E_g}\right)(\varepsilon)} \tag{46}$$

and

$$k = \sqrt{\frac{2m_o^*}{E_g} \frac{E_g{}'}{E_g} \left(1 + \frac{2\varepsilon}{E_g{}'}\right)(V - \varepsilon)} \tag{47}$$

To find numerical values for a comparison to the experimental results, values for E_g, t_o, $m_{\ell o}$, V_v and V_c must be determined. Assuming the difference, ΔEg between E_g and $E_g{}'$ given in equation (1) is split evenly between V_v and V_c then

$$V_v = V_c = 49.5 \text{ meV} \tag{48}$$

Formulas have been developed for E_g, $m_{t_{c,v}}$ and $m_{c,v}$ (at E=0) which depend on the temperature, T (in °K), such that[15]

$$E_g(T) = 171.5 + \sqrt{(12.8)^2 + .19 \ (T + 20)^2} \qquad \text{(meV)} \tag{49}$$

[15] H. Preier, "Recent Advances in Lead-Chalcogenide Diode Lasers," Applied Phys. 20, p. 189-206 (1979).

$$m_{t_C}(T) = m \left(30.58 \frac{E(o)}{E(T)} + 14.29\right)^{-1} \tag{50}$$

$$m_{t_V}(T) = m \left(30.58 \frac{E(o)}{E(T)} + 10.00\right)^{-1} \tag{51}$$

$$m_{\nu_C}(T) = m \left(\frac{30.58}{10.25} \frac{E(o)}{E(T)} + 2.42\right)^{-1} \tag{52}$$

$$m_{\ell_V}(T) = m \left(\frac{30.58}{10.25} \frac{E(o)}{E(T)} + 1.25\right)^{-1} \tag{53}$$

where m is the free electron mass equal to 9.11×10^{-31} kg. The thermistor temperature when the experimental data was taken at 82°K. At T = 82°K the above formulas and equation (13) yield

$$E_g = 217.8 \text{ meV} \tag{54}$$

$$m_{C_o}^* = .03485 \, m \tag{55}$$

$$m_{V_o}^* = .03930 \, m \tag{56}$$

Substituting the above values along with the value for V from equation (48) into the definitions of k and k' given in equations (46) and (47). We can solve equations (32) and (33) for ε_{C_n} or ε_{V_m}. The subscripts n and m refer to the energy levels in the conduction and the valence band wells respectively. The energy of the interband transitions between these levels is

$$\varepsilon_{C_n V_m} = \varepsilon_{C_n} + \varepsilon_{V_n} + E_g \tag{57}$$

Using equation (57) with the solutions from equations (32) and (33) the various possible lasing transitions can be computed. In Table 2 the results of such calculations are shown. The first column identifies the energy levels involved in the laser transition. The second column lists the actual data (see Figure 26) for a diode current of 160 mA. The third, fourth, and fifth columns list the calculated frequencies of the lasing transitions for different values of temperature and

Laser Transition $\varepsilon_{c_n v_m}$	Observed Frequencies (cm^{-1}) 160 mA	Calculated Frequencies		
		(cm^{-1}) T=82°K $.5 \approx \dfrac{V_c}{V_c+V_v}$	(cm^{-1}) T=82°K $.87 = \dfrac{V_c}{V_c+V_v}$	(cm^{-1}) T=82°K $.87 = \dfrac{V_c}{V_c+V_v}$
ε_{11}	1902.5	1865.4	1855.1	1901.0
ε_{12}	1967.8	1992.1	1919.8	1965.9
ε_{21}		2001.6	2008.0	2052.9
ε_{22}	2117.9	2128.4	2072.8	2117.7

Table 2. The actual laser frequencies compared to the theoretical values at different temperatures and ratios of V_c to $(V_c + V_v)$.

different ratios of V_c to $(V_c + V_v)$. The ratio of V_c to $(V_c + V_v)$ can be adjusted since only the total, $(V_c + V_v)$ is known (see equation (1)). In the third column the frequencies were obtained using $V_c = V_v$ or a ratio of $V_c/(V_c + V_v)$ equal

to .5. In the fourth column, the ratio of $V_c/(V_c + V_v)$ was adjusted to .87 in order to obtain separations between ε_{11} and ε_{11} which were closer to the observed values. Though the calculated frequency separations are close to the observed values, the frequencies listed in the fourth column are on the low side. The calculated frequencies can be increased if it is assumed that the diode temperature in the active region is higher than the measured thermistor temperature. A difference in the two temperatures is possible since the thermistor is mounted on the heat sink (see Figure 4) away from the diode which carries a current density of about 3 kA/cm^2 at 150 Hz. In addition, at these temperatures, a small error of the order of 2.5% in the voltage drop across the thermistor will result in a temperature error of more than 5°K. Even with both of the above errors, the 14°K increase in the diode temperature required to fit the data seems unreasonably high. This high temperature and the fact that the transition ε_{21} is not present in the data indicates that the simple model considered here may not be quite adequate.

In addition to the large separations in frequencies examined above, smaller average separations between frequencies were also observed. For laser diode No. 4 at 13°K, there was an average separation, $\overline{\nabla \nu}_1$, of 1.77 cm^{-1} (see Figure 19). This separation is most likely equal to the difference between longitudinal modes in the laser cavity. The separation between longitudinal modes is[16]

---

[16] Equations (58) and (59) derived from formulas in G.H.B. Thompson, Phys. of Semiconductor Laser Devices (Wiley 1980) p. 118.

$$\overline{\Delta \nu} = \frac{1}{2n_g d} \tag{58}$$

where d is the cavity length and n_g is the group refractive index given by

$$n_g = n - \lambda \frac{dn}{d\lambda} \tag{59}$$

Using equation (58) and the cavity length, d = 355 μm, for diode No. 4 the average mode separation of 1.77 cm^{-1} yields a group refractive index, n_g, of 7.96 for $Pb_{.84}Sn_{.16}Te$. The larger average separation, $\overline{\nabla \nu}_2$, of 11.4 cm^{-1} and 12.5 cm^{-1} for diodes No. 4 and No. 5, (see Figures 19 and 25) respectively, probably indicates a transverse mode possibly related to gain or current density quiding in the plane of the p-n junction.

I have not attempted to explain the magnetic field behavior of the laser diodes. It is my hope that the data obtained herein will stimulate others to undertake this interesting task, as well as to reexamine the quantum well theory with more accurate model.

Appendix A. Thermistor Calibration

With the Thermistor Submerged in	T°K	Readings (μV) +	Readings (μV) −	
Air	300	31.0	30.5	30 μV scale
Liquid Nitrogen	77	44.0	43.5	100 μV scale
Liquid Nitrogen	4.2	1240	1230	3 μV scale

Table A1. Calibration Points for the Thermistor

Equation to be fit [17]

$$\log R/T = a + b(\log R) + c(\log R)^2 \qquad (A1)$$

where R = thermistor resistance; T = temperature in K°

The thermistor resistance is calculated using:

$$R = \frac{V_R(29.81)}{V_{Battery} - (V_R)(10^{-6})} \qquad (A2)$$

where V_R = the voltmeter reading across the thermistor in μV.

$V_{Battery}$ = voltage of battery in thermistor circuit (Figure 5).

29.81 = resistance of current limiting resistor in mega-ohms (Figure 5).

1. Using the average between the plus and minus readings in the table above in equation (A2) the average thermistor resistance was found for each temperature.

---

[17] J.P. Frank and D.L. Martion Can. J. Phys. 39 1320 (1961) and D.H. Borcherds, Rev. Sci. Instrum. 9 138 (1969).

Appendix A   (continued)

2. Putting the average thermistor resistance and the corres-
    ponding temperature in equation (A1) yielded 3 equations,
    one for each temperature.

3. Solving these three equations simultaneously the 3 un-
    knowns (a,b, and c) were found

$$a = 4.7325 \qquad b = -1.6108 \qquad c = .13662$$

4. Thus using equation (A2) to find the resistance across the
    thermistor and plugging that into equation (A1) with a, b,
    and c above yields the temperature T, of the thermistor.

Appendix B. The Current Source

The current source for the laser diodes used in this experiment was designed and built specifically for this experiment by Yehuda Golahny of Francis Bitter National Magnet Laboratory. The current source has the following features.

1. A square wave output which cycles between 0 and some set current level.

2. A square wave frequency range from 30 to 150 Hz (always set at 150 Hz during this experiment).

3. A synchronization output for a lock in amplifier.

4. Internal current level control from 0 to 100% of current range.

5. External current level input (attached to sweep unit).

6. Three current ranges — 0 to 10 mA, 0 to 100 mA, and 0 to 1000 mA, max.

A schematic of the current source is shown in Figure B2 but a simpler block diagram, shown in Figure B1, illustrates the operation of the current source. From the current level control section of a voltage, which was either internally generated or externally supplied, was applied via switch 1 to a voltage controlled current source. Switch 1 was opened and closed in response to a square wave control signal from the frequency generator which was set to a frequency of 150 Hz during this experiment. This caused the voltage out of switch 1 to
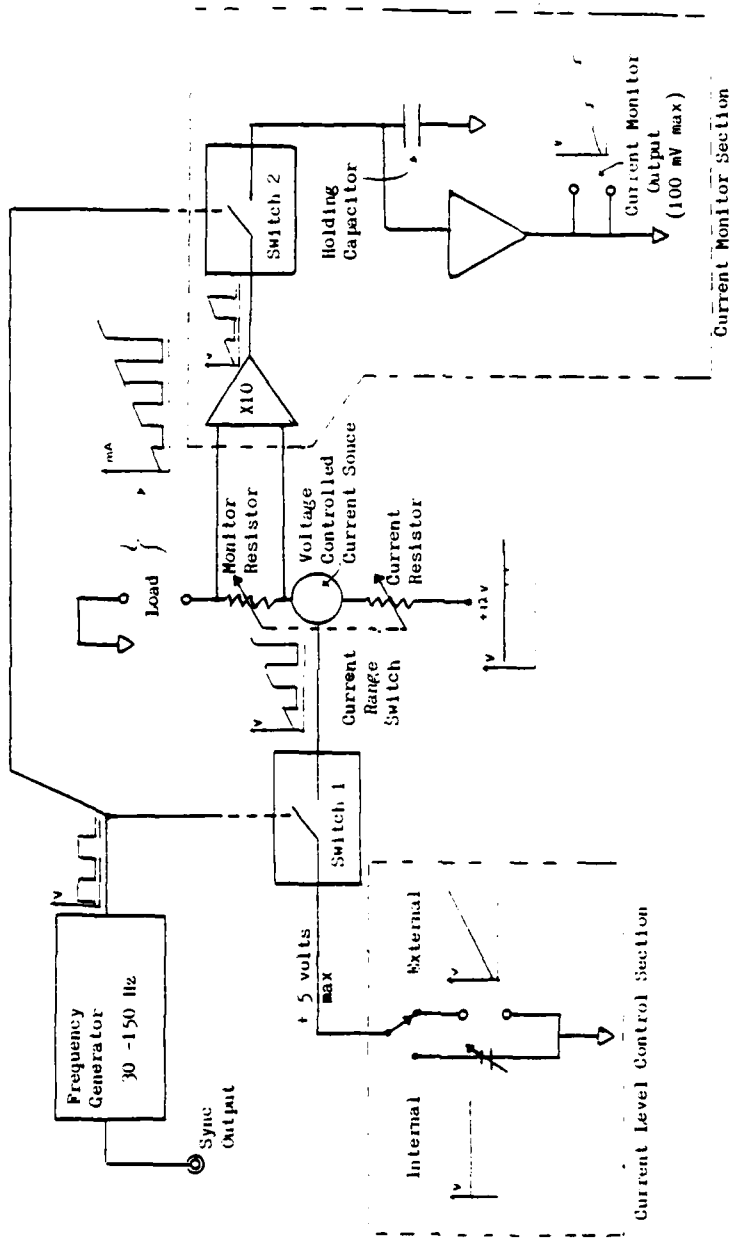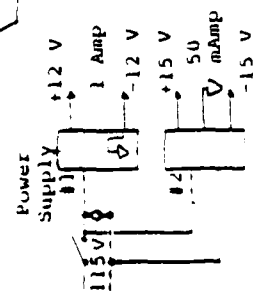
77

Figure B1. Block diagram of current source

Figure B2. A schematic of the current source.

oscillate (at 150 Hz) from 0 (with switch open) to the voltage applied to switch 1 (with switch closed) by the current level control section. The oscillating voltage from switch 1 drove the voltage controlled current source causing it to produce a square wave of current which cycled from 0 current to a current directly proportional to the voltage input. The amount of current produced for a given input voltage depended on the current range selected, such that at the maximum input voltage of 5 volts, the peak current out was adjusted to be either 10 mA, 100 mA or 1 A. The voltage drop across a monitor resistor, in series with the load, was amplified by a factor of 10 and applied to switch 2. Like switch 1, switch 2 was also controlled by the frequency generator. During the on 1/2 cycle switch 2 was closed applying the current monitor voltage to a holding capacitor. During the off 1/2 cycle switch 2 was opened and the holding capacitor maintained the monitor voltage. The capacitor voltage was applied to a high input impedence amplifier which buffered the capacitor while presenting a low output impedence for current monitoring. The current monitor output was designed to provide a constant voltage up to 100 mV maximum when the current output was at full range.

The current source was calibrated using a voltage comparison unit (Tektronix Type W plug in unit) on a Tektronix Type 547 oscillascope. The peak to peak voltage

across a standard resistor connected to the current source was compared to the voltage set in the voltage comparison unit and the current level was adjusted until they were equal. The voltage from the current monitor output was measured on a digital voltmeter and tabulated. Several different currents were measured for each current range. A sample calibration sheet is shown in Table B1.

Current Supply Calibration

Standard Resistor	Current Range	Current (mA)	Comparison Voltage (mV)	Monitor Voltage (mV)
100	.01 A	0.00		0.000
		2.00	20.0	20.094
		4.00	40.0	40.180
		6.00	60.0	60.327
		8.00	80.0	80.420
		10.00	100.0	100.529
10	.1 A	0.0		-0.005
		20.0	20.0	19.880
		40.0	40.0	39.774
		60.0	60.0	59.712
		80.0	80.0	79.600
		100.0	100.0	99.580
1	1A	0		-0.003
		200.0	20.0	19.760
		400.0	40.0	39.532
		600.0	60.0	59.290
		800.0	80.0	79.090

Table B1. A sample calibration sheet for the current source showing the monitor voltage at various currents in each of the three current ranges. The standard resistor plugged into the current source for each range and the voltage set into the voltage comparison unit are also shown.

Appendix C. Spectrometer Calibration

When the Spex 1680B Spectramate was first used in the experiment gratings with 75 groves/mm and a blaze wavelength of 10 μm were installed and roughly aligned. In order to calibrate the Spectramate the radiation from a mercury lamp was split into spectral lines using a Perkin Elmer 99 grating spectrometer and directed into the entrance slit of the Spex 1680B Spectramate (1680B). An EGG silicon photodiode (Model SGD-444) was placed at the exit slit of 1680B. The detected signal was amplified using a lock in amplifier and recorded on a strip chart. The 1680B was set so that it would scan through one of the orders (m = 17 to 22) of reflection of the mercury line entering the 1680B. A scan was started simultaneously with the strip chart drive. When the 1680B scanned through the mercury line a peak was formed on the chart. By measuring from the start scan point to the center of this peak and using the scan and stripe chart speeds, the dial reading of the peak could be obtained. The dial on the 1680B only reads correct wavelengths if gratings with 1200 groves/mm are installed. The dial readings of the peaks had to be converted to readings corresponding to gratings with 75 groves/mm. The fundamental grating equation listed in the Spex Instruction[18] manual is

$$m\lambda = d(\sin \alpha + \sin \beta) \tag{C1}$$

---

[18]1680 Spex manual p. 4.

where

    m = order of reflection
    λ = wavelength
    d = grating spacing
    α = angle of incidence
    β = angle of diffraction

Since the dial records the actual wavelength (m=1) with d_{1200} = 1/1200 mm/grove, the wavelength of the radiation passing through the 1680B with d_{75} = 1/75 mm/grove is given by

$$\frac{m\lambda}{d_{75}} = \frac{(1)\lambda_{dial}}{d_{1200}} = \sin \alpha + \sin \beta \qquad (C2)$$

or

$$\lambda = \frac{d_{75}}{d_{1200}} \frac{\lambda_{dial}}{m} = \frac{16\ \lambda_{dial}}{m} \qquad (C3)$$

Using equation (C3) with the appropriate order number, m, the dial readings of the peaks could be compared to the wavelengths of the mercury line entering the spectrometer by converting the dial readings the peaks to wavelengths or by converting the mercury line wavelengths to dial readings. I choose to do the latter and Table C1 shows the data from a calibration run.

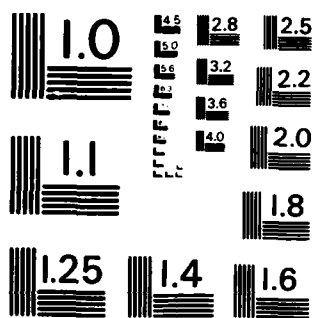MICROCOPY RESOLUTION TEST CHART

NATIONAL BUREAU OF STANDARDS-1963-A

Mercury Wavelength[19] in Air (nm)	Dial Reading (nm)	Dial Reading of Measured Peak (nm)
546.056	614.313	$617.973 \pm .05$
576.937	612.995	$616.659 \pm .05$
579.046	615.237	$618.891 \pm .01$
435.839	599.251	$602.950 \pm .06$

Table C1. Calibration data for Spex 1680B using the spectrum from a mercury lamp.

The dial readings of the peaks in the last column of the table are the averages of several scans. The error in the *average is the difference* between the average value and the value of the peak farthest from the average value. The actual error in the readings includes the errors in the scan speed ($\pm .18\%$) and the chart speed ($< .06\%$) plus any errors induced by not starting the scan and the chart simultaneously (probably $< .5$ sec). These errors yield a typical error of about $\pm .06$ nm in dial readings at the speeds used in calibration. The difference between the average dial readings actually observed and the correct dial reading for that line of mercury was converted to an error in the alignment of the gratings. This was

[19] From table of wavelengths using $n_{air} = 1.003$, presented in S. Zwerdling, J.P. Theriault, "Calibration of Prism Spectrometers in the Ultraviolet, Visible and Near Infrared Regions", Lincoln Laboratory Report 84G-0012, Figure 3 (July 27, 1960).

accomplished by assuming the errors in both of the gratings could be lumped into one grating (the other assumed to be correctly aligned) which is shown in Figure C1(a) and which follows equation (C1). The angles α and β are the actual angles of incidence and diffraction measured from the actual normal to the grating, the uppermost dark line. The light line is the position the normal would be in if the dial reading were set to what it should be for that mercury line. Thus

$$\alpha = \alpha H_g + \varepsilon \qquad (C4)$$

where

α = observed angle

H_g = the angle if the dial read correctly

ε = error in alignment

In order to convert the differences in reading shown in Table C1 to an error, ε, in the angle α, the angle $\underline{\beta}$ was eliminated from (C1) using

$$\beta = 2\theta + \alpha \qquad (C5)$$

where 2θ, as shown in Figure C1(a), is the fixed angle between incident ray and diffracted ray. By measuring the distances shown in Figure C1(b) the angle θ was determined to be 15.2°. Plugging (C4) and (C5) into (C2) with $\theta = 15.2^\circ$ and expanding the sines and cosines yields equation
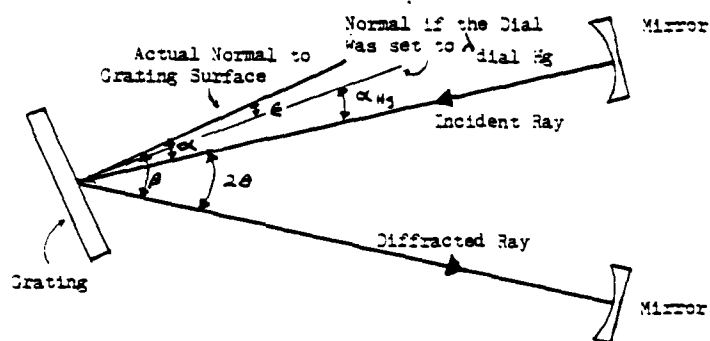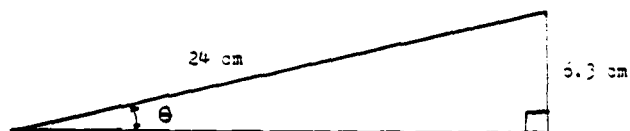
(a)   The grating arrangement

(b)   The measurements used to calculate θ

Figure Cl.   In (a) one of the two gratings in the 1680B
             is shown along with the various angles used
             in calibration calculation. In (b) the fixed
             angle θ is shown with the measurements used
             to calculate it.

(6) with the assumption that ε is small.

$$\varepsilon = \frac{\Delta\lambda_{dial}}{d_{1200}} \{\sin(30.4)\cos\alpha_{Hg} - [1+\cos(30.4)]\sin\alpha_{Hg}\} \quad (C6)$$

To use equation (C6) however, αHg must be determined. Using equation (C2) with (C5) and the following additional substitutions,

$$x = \sin\alpha\,H_g \quad (C7)$$

$$\sqrt{1-x^2} = \cos\alpha\,H_g \quad (C8)$$

$$y = \frac{\lambda_{dial\ of\ mercury}}{d_{1200}} \quad (C9)$$

$$a = \sin 30.4 \quad (C10)$$

$$b = 1 + \cos 30.4 \quad (C11)$$

yields

$$y = a\sqrt{1-x^2} + bx \quad (C12)$$

Solving for x in terms of y yields

$$x = \frac{\frac{yb}{a^2} \pm \sqrt{(\frac{by}{a^2})^2 - (\frac{b^2}{a^2}+1)(\frac{y^2}{a^2}-1)}}{(\frac{b^2}{a^2}+1)} \quad (C13)$$

(The minus sign gives the values appropriate to the actual physical situation.) With equations (C13) and (C7) they can be found

and plugged in equation (C6) to get ε.

Table C2 shows the error in dial reading, $\Delta\lambda_{dial}$, and the corresponding error in α, ε. The average error, $\bar{\varepsilon}$, equaled 2.46×10^{-3} radian . This average value could then be used to correct the dial readings of the laser radiation measured in this experiment.

Mercury Wavelength In Air (nm)	$\Delta\lambda_{dial}$ (nm)	ε (radians x 10^{-3})
546.056	3.660	2.462
576.937	3.664	2.464
579.046	3.654	2.459
435.839	3.698	2.464

Table C2. A list of the difference between the observed and correct dial reading and the corresponding alignment error for each of the mercury lines.

Appendix D. Quantum Well Structure

The figures D1 and D2 are the structure charts on diode No. 5 and diode No. 6. The upper half of the charts shows the concentration of dopant used. The dotted line portion to the left of the quantum well at 4.5 μm is doped with Bismuth donors and the solid line to the right is doped with Thallium acceptors. The lower half of the charts show the percentage of Europium in the $Pb_{1-x}Eu_xSe_yTe_{1-y}$ confinement layers. The charts were provided by Dr. Dale Partin who also provided the laser diodes.
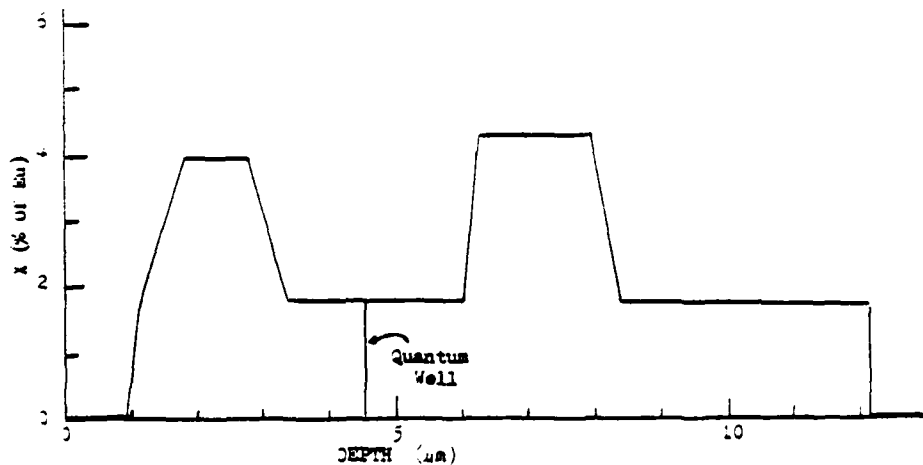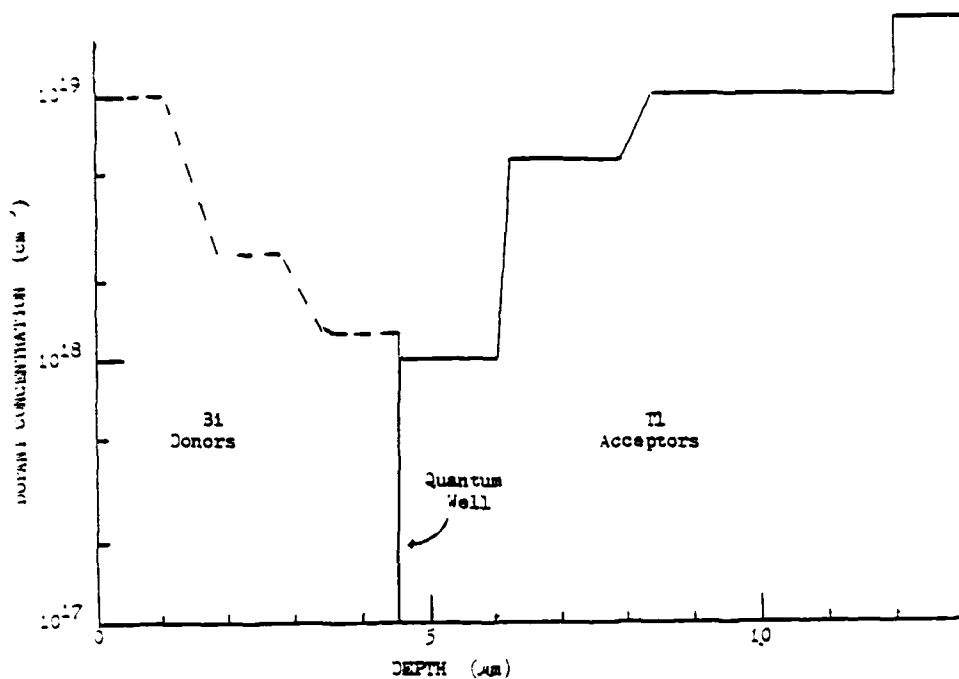
gure D1. Diode No. 5's structure. The upper shows the
          dopant concentration and materials. The
          lower chart shows the percentage of Eu in the
          $Pb_{1-x}Eu_xSe_yTe_{1-y}$ confinement layers.
          The PbTe quantum well thickness is 300 A and
          it was not intentionally doped.
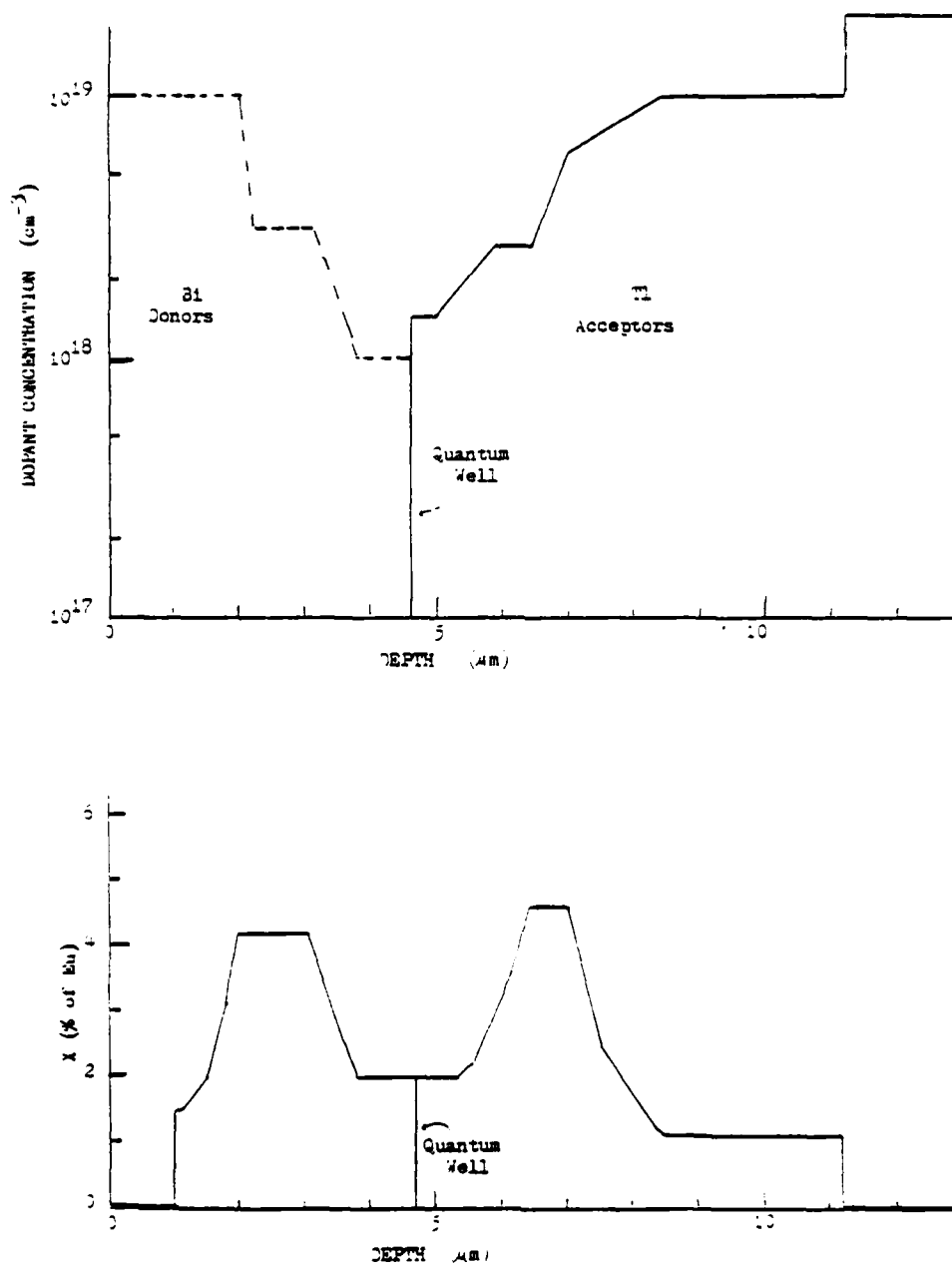
Figure D2. Diode No. 6's structure. The upper chart shows the dopant concentration and material. The lower chart shows the percentage of Eu in the $Pb_{1-x}Eu_xSe_yTe_{1-y}$ confinement layers. The PbTe quantum well thickness is 600 A and it was not intentionally doped.